UNIVERSITY OF MIAMI

TEMPORAL FLUCTUATIONS OF THE SOUND SPEED FIELD AND HOW THEY AFFECT ACOUSTIC MODE STRUCTURES AND COHERENCE

By

Felipe Messias G. Lourenço

A THESIS

Submitted to the Faculty
of the University of Miami
in partial fulfillment of the requirements for
the degree of Master of Science

Coral Gables, Florida

December 2012

UNIVERSITY OF MIAMI

A thesis submitted in partial fulfillment of
the requirements for the degree of
Master of Science

TEMPORAL FLUCTUATIONS OF THE SOUND SPEED FIELD AND HOW THEY AFFECT ACOUSTIC MODE STRUCTURES AND COHERENCE

Felipe Messias G. Lourenço

Approved:

_____
Harry A. DeFerrari, Ph.D.
Professor of Applied Marine Physics

_____
M. Brian Blake, Ph.D.
Dean of the Graduate School

_____
Jorge F. Willemsen, Ph.D.
Professor of Applied Marine Physics

_____
Arthur J. Mariano, Ph.D.
Professor of Meteorology &
Physical Oceanography

_____
Kevin B. Smith, Ph.D.
Professor of Physics
Naval Postgraduate School

LOURENCO, FELIPE MESSIAS G. (M.S., Applied Marine Physics)

Temporal Fluctuations of the Sound Speed Field and How They Affect Acoustic Mode Structures and Coherence (December 2012)

Abstract of a thesis at the University of Miami.

Thesis supervised by Professor Harry A. DeFerrari.
No. of pages in text. (67)

In an idealized shallow water propagation channel with smooth boundaries and range independent sound speed profiles, normal modes can accurately describe the entire sound field which can be predicted using normal mode models.

We also know that fluctuations in the sound field can be caused by fluctuations in the sound speed profile or by source/receiver motion. These phenomena are deterministic and can be simulated by changes in the mode shape or by a combination of the motion of modes past the receiver. If the fluctuations are small then small changes will occur in the mode shape or in the mode positions, hence the phase response will be approximately linear and our propagation is “phase coherent” relative to the background noise. Furthermore, spatial and temporal averaging is possible, which enhances the signal-to-noise ratio (SNR). But random fluctuations of the sound speed caused by multipath interactions with the boundaries can totally distort the acoustic modes reducing and sometimes annihilating phase coherence.

The research community seeks to understand the effects of internal waves on temporal coherence and a considerable number of experiments using fixed system to observe both oceanographic and acoustic fluctuations has been conducted.

On the other hand, the applied Navy is more concerned with mobile platforms and underwater communications in which spatial coherence is measured instantaneously. Thus, the long term temporal coherence observed by basic research has little interest to mobile platforms.

In this work we seek to understand coherence in terms of the normal acoustic mode structure. This structure can be randomized by fluctuations of the sound field and fluctuations of the boundaries. The research proposed here emphasizes the temporal fluctuations of the sound speed profile and how they affect acoustic mode structures and coherence. To achieve that, the MMPE (Monterey-Miami Parabolic Equation) model will be used to predict the mode shapes in a range dependent channel and random fluctuations will be introduced to observe how the modes are distorted in space and time. In turn, we can use these mode structures to estimate the temporal and spatial coherence of the mode arrivals allowing us to compare predictions of coherence for individual acoustic modes with observations.

Dedication

I dedicate this thesis to my wife Camila and my daughter Manuela, for their unconditional love and support that guided me throughout this journey.

Acknowledgements

I would like to thank my advisor/chairperson of my committee Dr. Harry DeFerrari for his support, comments, patience and guidance during this entire work. I also thank my other committee members: Dr. Jorge F. Willemsen and Dr. Arthur J. Mariano for their support and comments and Dr. Kevin B. Smith, Professor of the Naval Postgraduate School, for his support, thoughtful comments and also for providing the codes to be used in this work. I would like to thank Jennifer Wylie for her amazing help with the codes, comments, suggestions and reviewing this thesis; Fernando Monteiro for his support, suggestions and the insightful discussions about my research topic. I'm also grateful to the faculty, staff and students (especially my classmates) in the Division of Applied Marine Physics. I also gratefully appreciate the sponsorship given by the Brazilian Navy and the guidance of my Navy's advisors Captain Marcus Simões and Captain Alenquer.

Finally, but most importantly, my family. Leonor, Paulo and Yasmin for their endless support. Camila, my wife, and Manuela, my daughter for their unconditional love and my parents Ana and Manuel and my grandparents Joaquim and Thereza for their love, encouragement to go after my dreams, and for giving me the tools to achieve them.

TABLE OF CONTENTS

List of Figures

List of Tables

List of Acronyms/Abbreviations

AOCE	Acoustic Observatory CALOPS Experiments
ASIS	Air-Sea Interaction Spar
CIW	Continuous background Internal Wave
ENV	Environmental mooring
EOF	Empirical Orthogonal Function
FSPE	Florida Straits Propagation Experiments
HLA	Horizontal Line Array
IW	Internal Waves
MMPE	Monterey-Miami Parabolic Equation
MSM	Miami Sound Machine
PE	Parabolic Equation
SBE	Sea-Bird Electronics
SHRU	Single Hydrophone Receiving Unit
SIW	Solitary Internal Wave
SRBR	Surface-reflected-bottom-refracted
SSF	Split-Step Fourier
SSP	Sound Speed Profile
SW	Shallow Water
SW06	Shallow Water 2006 Experiment
Tpod	Temperature sensor
VLA	Vertical Line Array
WHOI	Woods Hole Oceanographic Institute

List of Symbols

COH	Coherence
cyc/day	Cycles per day
db	Decibel
ΔT	Experimental time
fft	Fast Fourier Transform
f(k)	Function f in the frequency domain
f(t)	Function f in the time domain
Hz	Hertz
ifft	Inverse Fast Fourier Transform
Km	Kilometer
M	Meter
Mi	Mile
min	Minutes
p(t)	Pulse response
s	Seconds
sec.	Seconds
t	Arrival time
T	Coherence lag time
SPL	Sound Pressure Level
W^{-2}	Decreasing frequency slope
W^{-4}	Decreasing frequency slope

CHAPTER 1

INTRODUCTION

1.1 MOTIVATION

The coherence in underwater acoustic signals implies phase and / or amplitude stability in space and / or time. This stability is used to achieve gain or enhancement of the signal above the ambient noise. Without coherence, signals resemble the noise background and therefore there can be no signal processing gain. Hence, SSP fluctuations and multiple interactions with the boundaries can affect this stability.

Internal waves are an important factor of vertical mixing in the ocean and they can have an effect on sound propagation in the water column. The influence of internal waves (IW) is more pronounced in the regions of ocean shelves, seamounts, and the continental slope. When passing over the shelf, the internal tide undergoes a nonlinear transformation which creates a train of short waves. These short waves travel towards the coast and produce local perturbations in the thermocline and the resulting sound speed profile (SSP). SSP variability along the path of propagation tends to reduce the coherence of signals. However, other factors also affect coherence such as source/receiver motion and variations of the sound channel and boundaries (surface and bottom). All of the variables combined will contribute to reduce the coherence in time and also in space.

In this thesis the coherence of each separate mode is analyzed. In this way multipath interference effects will be eliminated and a more detailed discussion of the parameters that affect coherence is possible. In all the cases presented here the bottom is held flat in order to study only the influence of fluctuations on the sound speed. Ideal flat

bottoms in shallow water propagation channels produce predictable surface-reflected-bottom-reflected (SRBR) mode structures that have predictable group velocities. Hence, arrival patterns for pulse transmissions can be identified by travel time.

To pursue the goal, the data from three shallow water experiments were analyzed to observe and compare coherence properties of individual mode arrivals in time. Mode coherence measures were systematically compared for different frequencies, mode numbers and channel parameters and for a variety of internal wave energy levels. A number of consistent trends and relations were observed. For example, lower order modes were more coherent than higher order modes especially at higher frequencies. Additionally, the first mode appeared almost unaffected by the channel sound speed fluctuations. Low frequency coherence is mostly determined by internal waves while high frequency coherence is limited by bathymetry fluctuations. Furthermore, both spatial and temporal coherence exhibit the same trends and relationships. Of note is the finding that the qualitative features of temporal and spatial coherence show the same dependence on frequency and mode number. This suggests the possibility of a single unified theory to predict temporal and spatial coherence using statistics of the internal wave field and bathymetry as inputs. Our research is pursuing this avenue with very encouraging results so far.

The first shallow water site selected for this work is located at about 160 Km east of the New Jersey coast where a large experiment was conducted: The Shallow Water 2006 Experiment (SW06). These data were collected over a broad range of frequencies and for a variety of oceanographic conditions such as different depths, bottom properties

and internal wave types. The SW06 site is characterized as a retrograde front, since the currents of the SW06 site block the IW propagating from the ocean.

Two other experiments were taken into account in this work: The Acoustic Observatory CALOPS Experiments (AOCE) and The Florida Straits Propagation Experiments (FSPE). These experiments were located in the Straits of Florida. Here we find a prograde front, i.e., the IW activity from the open ocean is able to propagate along the shelf resulting in an area more saturated of internal waves.

It's important to mention that all three experiments have consistent and comparable signal types and processing as well as they were designed to have separable and resolvable mode arrivals allowing the calculation of coherence for individual modes of propagation.

The modeling approach here is to use the Monterey-Miami Parabolic Equation (MMPE) to predict the mode structure which in turn will be interpreted by mode theory to further explain the results (Smith 2001). We hope to gain a better understanding of the system and how each variable affects the SSP and consequently the coherence.

Matlab was used as a tool to both process and model the data. By using different time and frequency filters to analyze the Power Spectral Density of various thermistors at different depths and moorings, we were able to investigate the temporal and spatial oscillations of the sound speed profile to determine at which sensor/sensors the most significant oscillation occurs/occur. Furthermore, the sound speed variations were broken up into distinct frequency bands. The temporal and spatial coherence of each band was studied in order to understand their contribution to the overall loss of coherence.

A complete and detailed description of the fluctuations of the entire sound speed field is beyond the capability of the PE models. Some simplifying assumptions are necessary. First, the only vertical fluctuations allowed are coherent; that is, they are in phase vertical displacements that are largest near the steepest part of the thermocline and smaller near the bottom and surface determined by fits to thermistor data. These are typically the lowest order modes of the internal wave field. Secondly, range dependant fluctuations are introduced using three range steps. The steps correspond to the locations of three thermistor moorings along the path of propagation.

Comparisons of results from different experiments were also made. An agreement between the model's prediction and observed data was clear. A consistent finding for all three propagation sites is the decrease in coherence with increasing mode number. Both spatial and temporal mode coherence exhibit the same trend suggesting the possibility of a unified theory or model that can predict both in terms of simple and intuitive mode coherence.

For low frequencies, <100 Hz, the bottom appears flat and under low internal wave activity perfect modes are formed and coherence time is hours - essentially unlimited coherent times for all modes. As internal wave energy along the propagation path increases the coherence time decreases to a few minutes for all modes.

For high frequencies, >800 Hz only the single lowest order mode is observed with coherence time of a minute even under very low internal wave energy. Higher order modes are smeared in space and time and have coherence time of less than a few seconds.

For the intermediate frequencies all modes are recognizable but higher modes are deformed and smeared so that higher order modes are less temporally coherent than lower order modes. The same trend is observed for spatial coherence.

Despite the high intense solitons observed during the experiment they do not affect the modes as originally thought and this effect for different bands of frequency is almost the same for all modes most of the time.

The work contained in this thesis is divided into four chapters. Chapter One contains the Motivation and Experimental Results, Chapter Two covers The Oceanographic Acoustic Environment and Model Inputs, Chapter Three is about the Data Analysis itself and finally in Chapter Four the results are summarized and there is a discussion about future work.

1.2 EXPERIMENTAL RESULTS

Data from the AOCE and FSPE experiments were analyzed in two papers: Temporal Coherence of Mode Arrivals (DeFerrari et al 2008) and Observations of low-frequency temporal and spatial coherence in shallow water (DeFerrari 2008). In this section, these experimental results will be shown and explained in order to provide a better understating of what is going to be done in this thesis. Figure 1.1 shows decreasing coherence for successive mode arrivals.

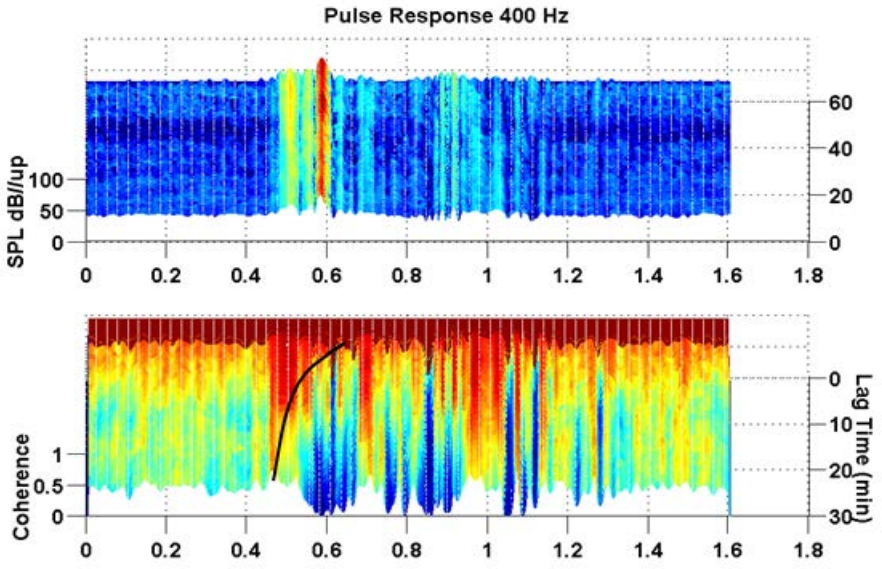

Figure 1.1: Decreasing coherence for successive mode arrivals.

The decrease in coherence with increasing mode number of the arrival is a consistent finding for all three propagation sites.

Figures 1.1 and 1.2 are for Florida Straits. These figures show a strong relation between mode number and coherence with higher mode successively less coherent than lower order at mid frequencies from 200 to 800 Hz.

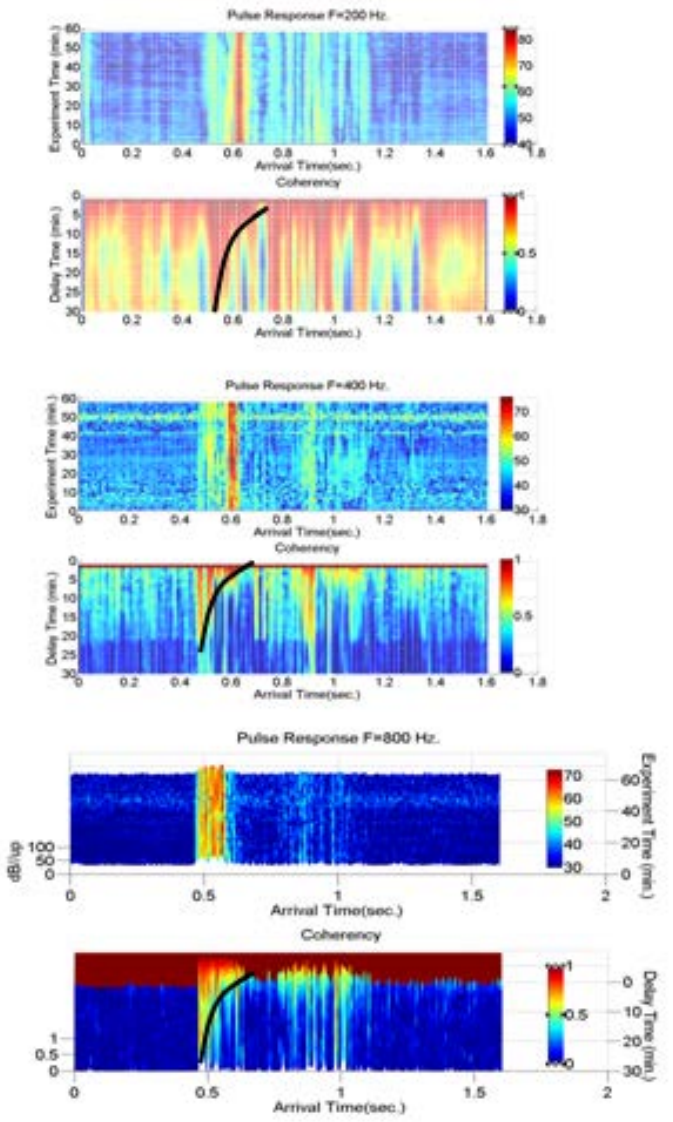

Figure 1.2 SRBR pulse arrivals and coherence for 200, 400 and 800 Hz transmissions in the Florida Straits.

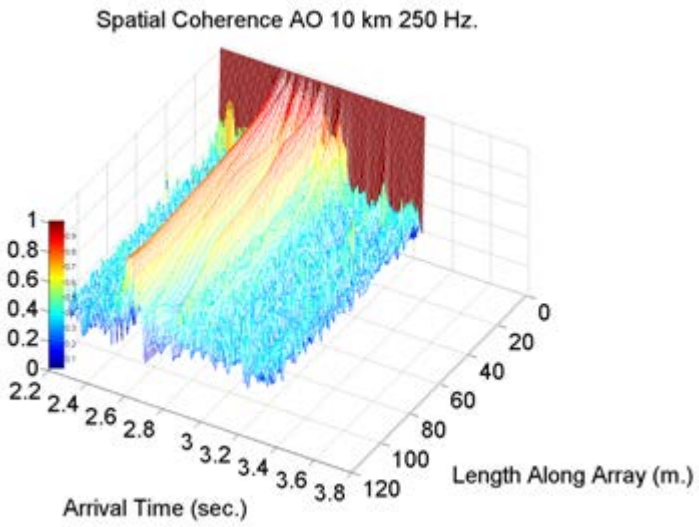

Figure 1.3: Spatial coherence for 6 mode arrivals computed from HLA perpendicular to the direction of propagation – Acoustic Observatory Data.

Figure 1.3 shows the same feature but the data are for spatial coherence along a 118 m array perpendicular to the direction of propagation. The data are from the acoustic observatory experiment with the source being suspended from a ship holding station. It is significant that both spatial and temporal mode coherence exhibit the same trend. As mentioned previously, this suggests the possibility of a unified theory or model that can predict both in terms of simple and intuitive mode coherence.

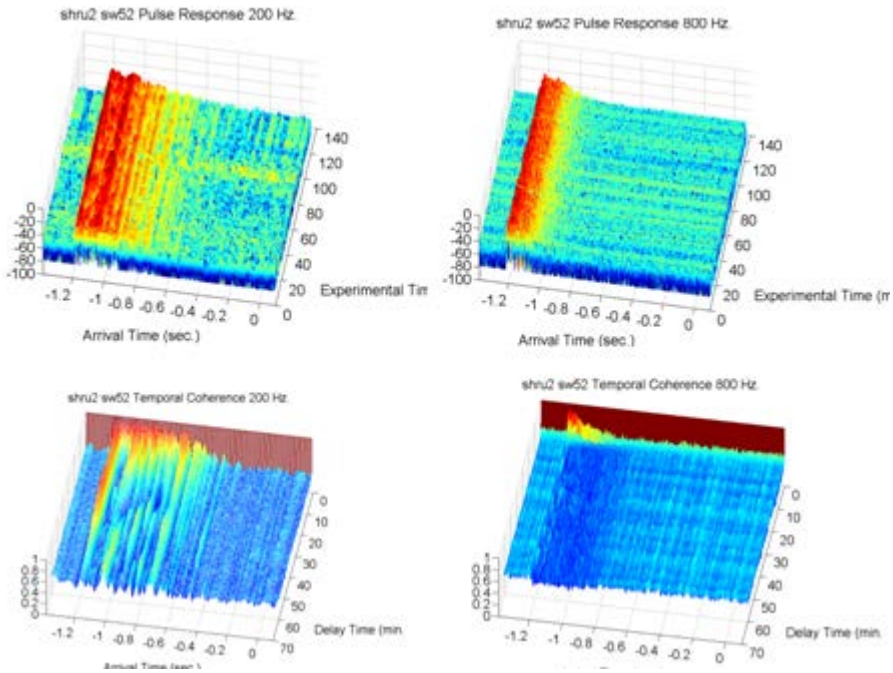

Figure 1.4: Pulse arrivals and Coherence from SW06 measurements for 200 and 800 Hz.

Fig. 1.4 shows the similar calculation for SW06 data. The New Jersey site data is about twice the range and 2/3 the depth that of the Florida Straits site. The trend is apparent and the same for the 200 Hz, but the coherent is much less for the 800 Hz data. Further we note that the discrete separable modes arrivals are not present for the higher frequency. Instead the arrivals are smeared together for a continuum of modes. The result is nearly a complete loss of coherence.

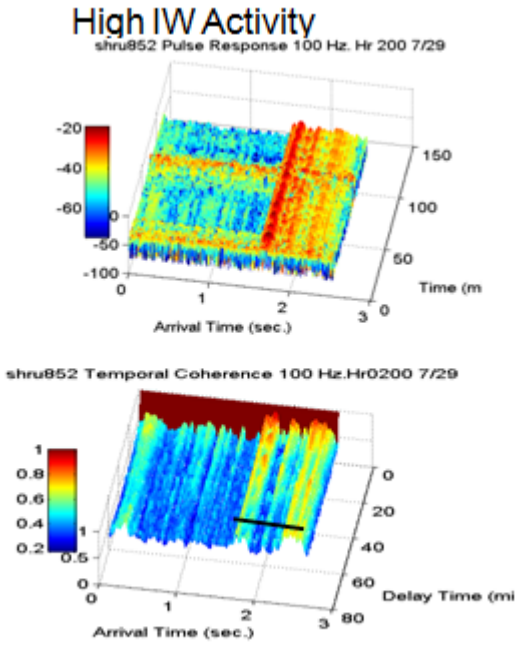

Figure 1.5: Pulse Arrivals and Coherence SW06 100 Hz during high IW energy.

The SW06 100 Hz data are not shown for the case of low internal wave energy. Nearly perfect coherence was observed. No change in modes in time was observed for periods of over an hour except for a slow translation in response to barotropic tides. However, during high internal wave periods, with the passage of solitary waves, the coherence drops of rapidly but for all modes equally unlike other higher frequency data discussed above (see Fig 1.5).

It became apparent early on the analysis that we could not account for the observations by of internal waves alone.

CHAPTER 2

METHODOLOGY

2.1 THE OCEANOGRAPHIC ACOUSTIC ENVIRONMENT

The data for the first experiment used in this thesis were collected in the summer of 2006 during a large multi-disciplinary experiment, the New Jersey Shelf Shallow Water 2006 (SW06) experiment. This work was conducted on the Mid-Atlantic Bight continental shelf at a location about 160 Km east of the New Jersey coast and about 80 Km southwest of the Hudson Canyon. The moorings were deployed in a "T" geometry creating an along-shelf track following an approximate 80 m isobath line and a cross-shelf track with depths from 50 m to 500 m as shown in figure 2.1.

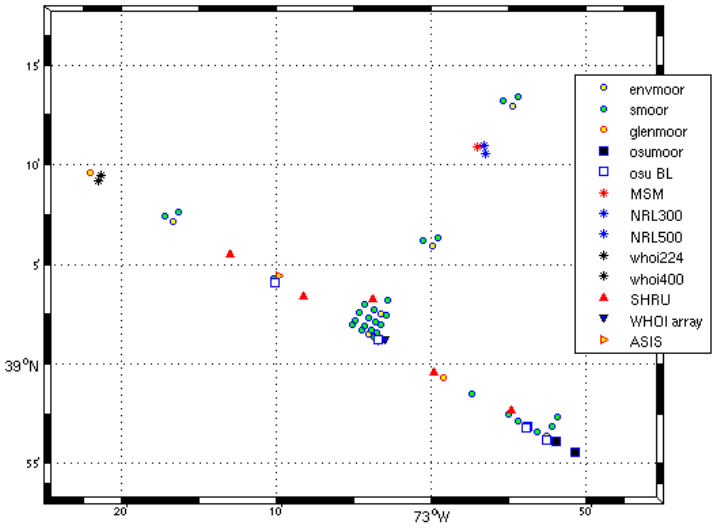

Figure 2.1: SW06 Chart with moorings and locations. Reprinted from Woods Hole Oceanog. Inst. Tech. rept., WHOI-2007-04.

This site is characterized by relatively flat bathymetry and regular periods of internal wave activity (IW), which are the result of the spilling of tidal current over the

shelf edge. These IW are timed with the tides (DeFerrari, 2008), which are the only source of IW activity since the currents of the SW06 site block the IW propagating from the ocean (retrograde front).

The schematics of The Acoustic Observatory CALOPS Experiments (AOCE) and The Florida Straits Propagation Experiments (FSPE) are presented in figure 2.2.

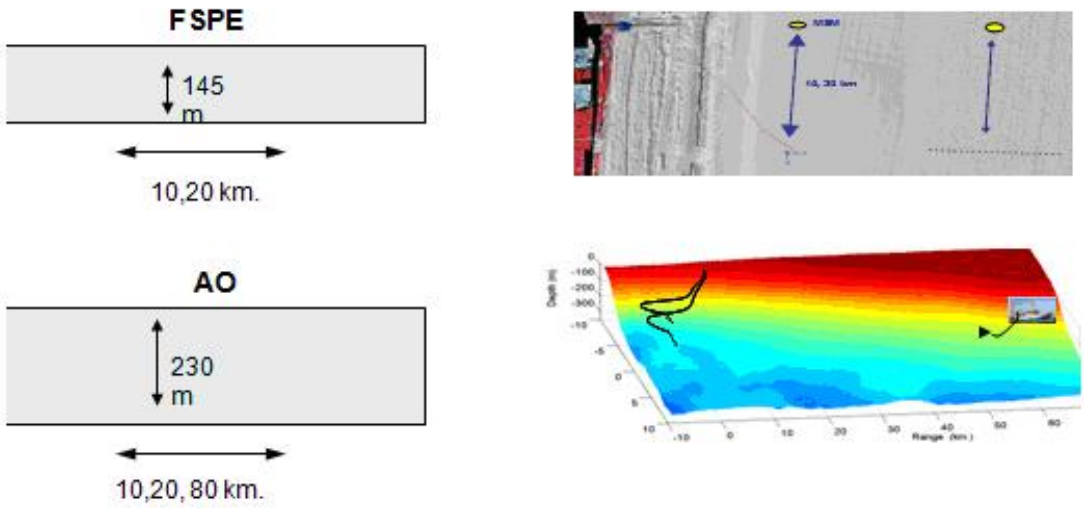

Figure 2.2: AOCE and FSPE experimental geometry.

The area where these experiments were conducted is also characterized by relatively flat bathymetry but is more saturated by internal waves.

The FSPE experiment was conducted at a depth of about 145 m and ranges between 10 and 20 Km using continuous transmissions allowing us to evaluate temporal properties of the signal.

The AOCE experiment used an array of elements located along the Miami terrace at a depth of about 230 m and ranges varying from 10, 20 and 80 Km using 20 minutes transmissions allowing us to calculate spatial properties from 20 to 80 Km. Both

experiments used multi-frequency broadband sources (e.g. MSM – Miami Sound Machine) to give good frequency coverage.

2.2 MONTERREY-MIAMI PARABOLIC EQUATION MODEL

The basic premise of the work is to relate coherence and mode structure. Earlier studies have found that coherence begins to deteriorate when mode structures break up beginning with higher-order modes. In this work the aim is to predict and calculate the temporal coherence for the individual modes. To predict the temporal coherence we will use time histories of the fluctuation for each mode arrival, which are going to be the result of the variation of the Sound Speed Profile (SSP) due to the passage of internal waves. The hope is to find new parameters to describe the coherence calculation.

In order to model and to predict the influence of the slow variation of the SSP, due to passage of IW's, on the mode shapes we will use the Monterrey-Miami Parabolic Equation (MMPE). The PE model was chosen because it is easy to use and handles range dependence much better than normal mode and ray tracing models. The former tends to be more computationally intensive whereas the latter is unstable and provides coarser results (caustics, bottom reflections, and diffraction corrections for bottom cutoff). In addition, ray tracing is best used in deep water and when working with higher frequencies since in those cases ray effects become more important than wave effects (Blatstein et al 1973).

The MMPE model is based on the split-step Fourier (SSF) algorithm that solves the parabolic equation by Fourier transform techniques and the program outputs can be

easily manipulated in Matlab. The input parameters are easily modified allowing us to make more calculations in a short time basis. Figure 2.3 exemplifies the algorithm.

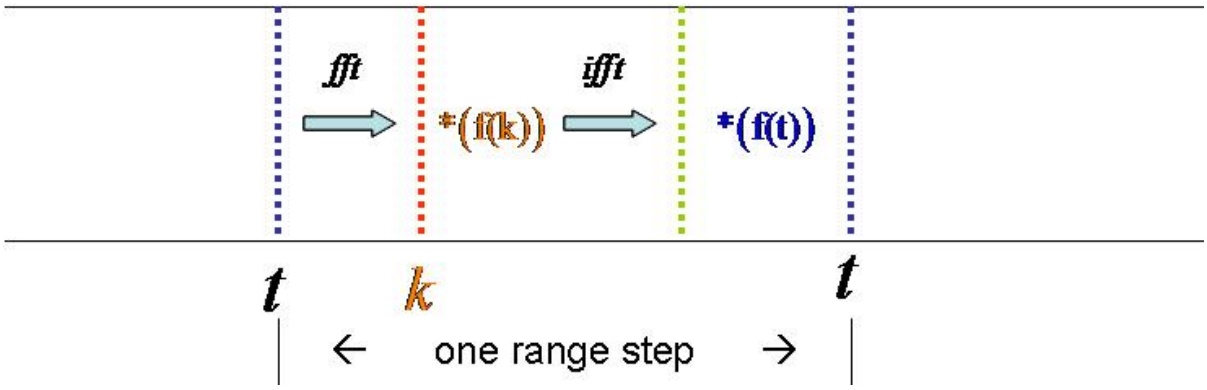

Figure 2.3: Split-Step Fourier Algorithm (Marching Solution).

2.2 SW06 DATA

The SSP acquired during the SW06 experiment will be used as the primary model input. This data is a statistical merging of data sources used to estimate the full water-column during the experiment (Y.-T. Lin et al 2006). An empirical orthogonal function (EOF) was used to merge overlapping profile data sets into a single time series of profiles. The data merged are from the WHOI VLA array, an air-sea interaction spar (ASIS) buoy and a nearby environmental mooring (ENV#30). The ENV#30 provided the temperature and salinity measurements used in the sound-speed conversion. The resultant profiles allow reliable mode decomposition, beamforming as well as modeling acoustic propagation. The sound speed profiles used in this work can be seen in figures 2.4 and 2.5.

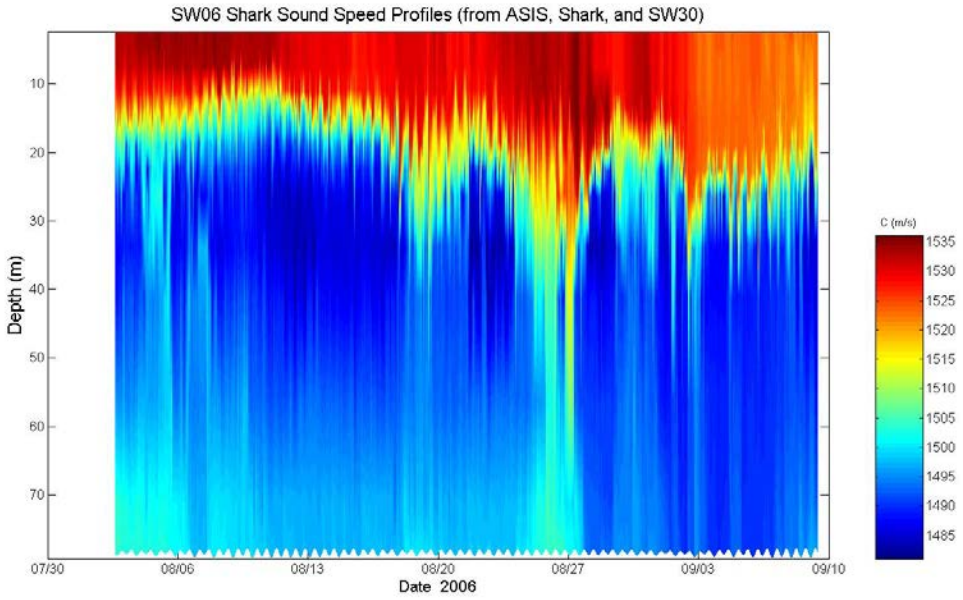

Figure 2.4: SW06 Shark Sound Speed Profiles (from ASIS, Shark and SW30). Reprinted from Woods Hole Oceanog. Inst.

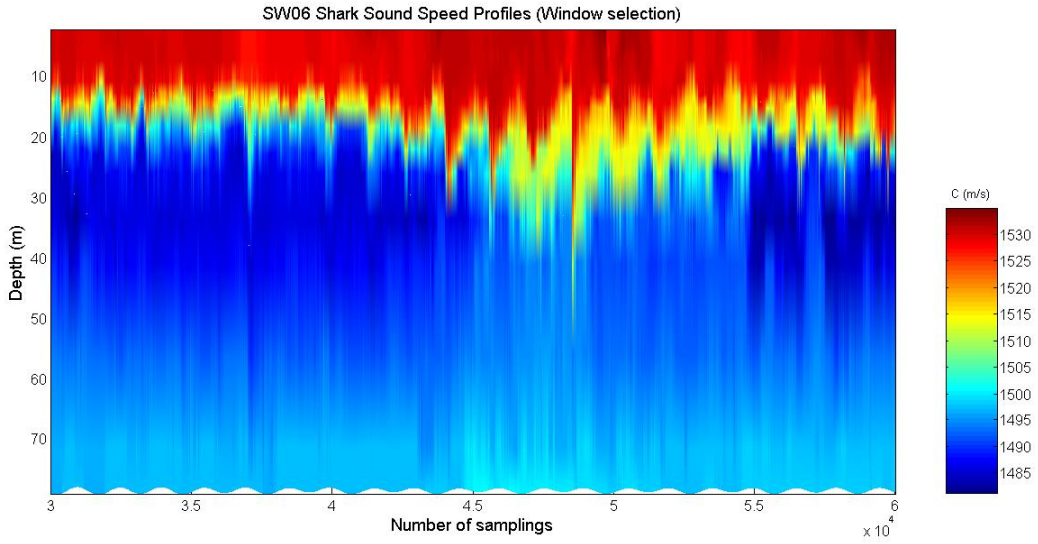

Figure 2.5: SW06 Shark Sound Speed Profiles – Window selection

A number of thermistors and one temperature/pressure sensor were attached to the VLA to get a time series of the temperature at the Shark mooring. The sampling interval of these sensors is 30 seconds and their depths can be seen in figure 2.6.

Sensor	Sensor Number	Depth (m) at deployment depth (79m)	Sampling interval (secs)
Tpod	2048	1	30
SBE39	242	13	30
Tpod	2047	15	30
SBE39	22	19	30
Tpod	2051	22	30
SBE39	23	26	30
Tpod	2096	34	30
Tpod	2097	41	30
Tpod	2094	56	30
Tpod	2095	71	30
Tpod	2062	79	30

Figure 2.6: Environmental sensors at Shark station – Reprinted from Woods Hole Oceanog. Inst. Tech. rept., WHOI-2007-04.

CHAPTER 3

DATA ANALYSIS

The data analysis is divided in the following four sections in order to provide clarity to the individual problems addressed. The first section discusses the Solitary Internal Waves (SIW) that are long regular wave trains with energy concentrated around a specific frequency. These are energized at regular intervals by tidal currents spilling over the edge of the shelf and then propagate shoreward over the propagation site. The second section addresses the raw data after some averaging. Third section will analyze the second type of IW: The Continuous background Internal Wave (CIW), which has spectral energy distributed over the entire internal wave spectrum. The forth section will show some model predictions for acoustic mode coherence using different filters, frequency bands and will also analyze the range dependence of coherence.

3.1 SOLITARY INTERNAL WAVE

This section analyzes the influence of the slow temperature variation due to the passage of internal waves. In order to study this slow variation we first selected a window from the original data. This window represents a period of time in which strong Solitary Internal Wave (SIW) activity is seen. To keep track of this variation figure 3.1 shows sound speed for mid-depth sensors (Sensors 5, 6, 7 and 8), which were chosen because their sound speed records show higher vertical fluctuations . After analyzing the time

series the power spectral density was computed for every thermistor as illustrated in figure 3.2. The slow temperature caused by SIW variation is timed with the tides and the tidal line is easily distinguishable on the PSD. Hence, a filter will be used to remove anything outside a range from tidal line leaving just the slow sound speed variations desired.

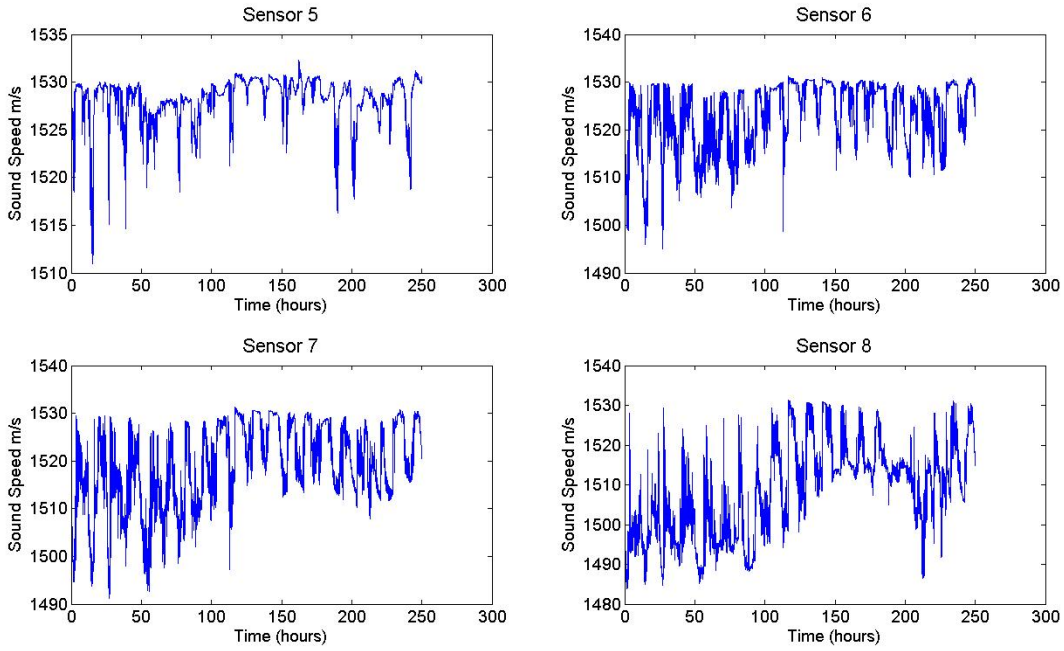

Figure 3.1: Time series from sensors 5 (22m), 6 (26m), 7 (34) and 8 (41m). This window has 10 days of data at a 30s sampling rate.

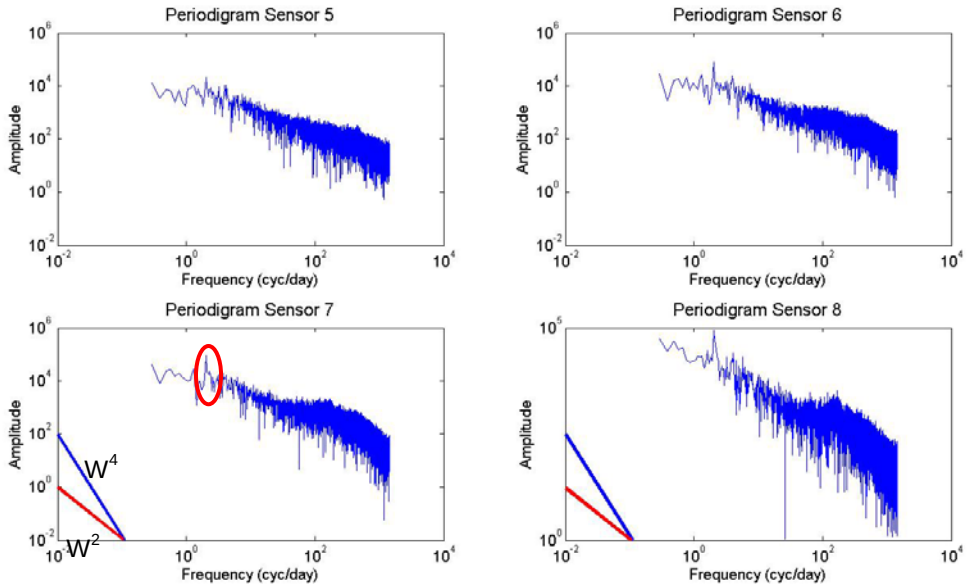

Figure 3.2: Log scale plot from sensors 5 to 8. In blue W^{-4} (the cut-off – Brunt–Väisälä frequency) and in red W^{-2}. The red circle shows the internal wave energy we are interested in (IW are timed with the tides).

As mentioned before, Matlab was used to filter the data allowing us to have a full water column SSP containing the slow temperature variation due to the IW activity as shown in figures 3.3 and 3.4.

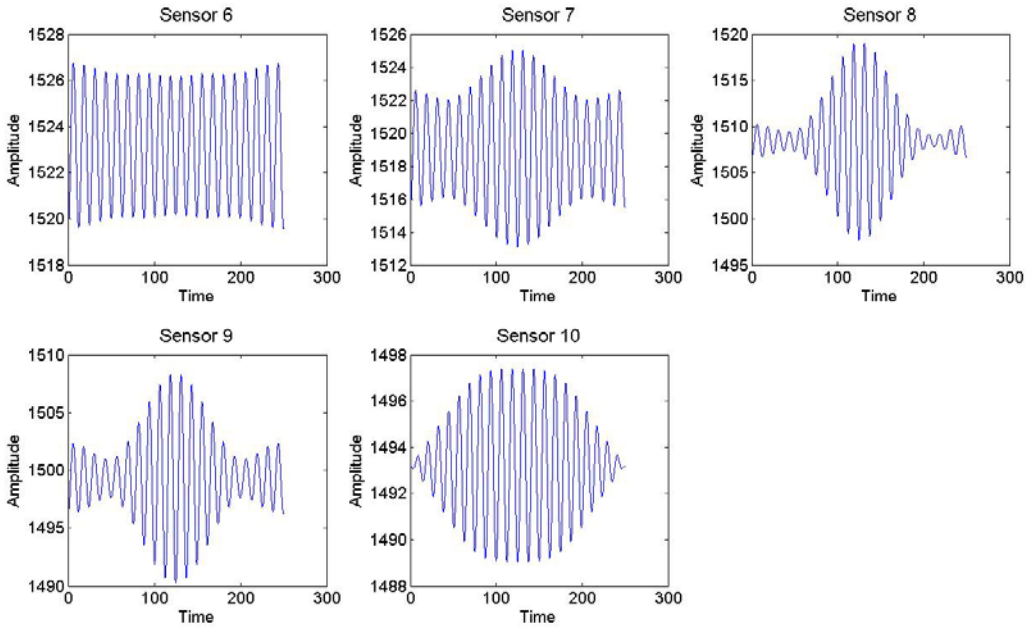

Figure 3.3: Time series of sensors 6, 7, 8, 9 and 10 after filtering for the SIW component.

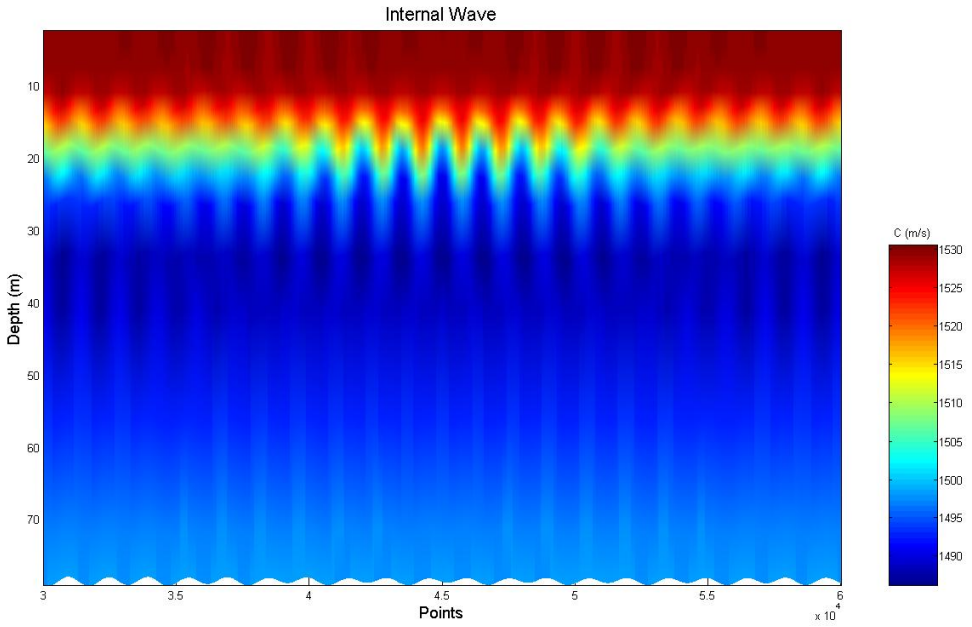

Figure 3.4: Same as figure 4 after filtering for the SIW component. Full water column SSP.

In order to isolate the effects due to IW activity, a flat bottom bathymetry profile will be used in all the modeling work. The full water column sound speed profiles

containing the slow variation of the temperature during the passage of the internal wave will be used as inputs to the MMPE model to predict the individual modes as a function of the arrival time. Using the model outputs, the temporal coherence of the individual modes will be calculated. Details of the calculation method have been described before (DeFerrari 2008). Temporal coherence is a complex quantity that depends on both phase and amplitude of the waveform and is computed as a normalized time lagged covariance function of the form:

$$\mathrm{COH}(t,\tau) = \frac{\langle (p(t)p(t+\tau))^2 \rangle_{\Delta T}}{\langle p(t)^2 \rangle_{\Delta T} \langle p(t+\tau)^2 \rangle_{\Delta T}},$$

In our equation p(t) is the pulse response, t the arrival time, ΔT the experimental time and T is the coherence lag time. Yet, here the lagged cross product of the equation above is computed on the time history section of p(t).

$$P(T,t) = \begin{vmatrix} \cdots\cdots p_{T=1}(t)\cdots\cdots \\ \tau \quad t \rightarrow \quad p_{T=2}(t)\cdots\cdots \\ \downarrow \quad\quad\quad p_{T=3}(t)\cdots\cdots \\ \cdots\cdots \\ \cdots\cdots \\ \cdots\cdots \\ \cdots\cdots p_{T=N}(t)\cdots\cdots \end{vmatrix}$$

The result is a value of coherence for every arrival time t at each coherence lag time T, which allows for the coherence for every individual mode to be analyzed.

3.1.1 RESULTS

As shown in figures 3.5 and 3.6, the first results were modeled using a two hour period during high internal wave activity while the results shown in figure 3.7 used only a

30 minute period. One sound speed profile was used for the entire 20Km range and then at every 30s a new SSP was used for the calculation. As mentioned before 30s is the resolution of our sensor. The mode structure presented is in depth and is only for one particular SSP; however the coherence was picked out at one depth for each SSP making the coherence results comparable to the SW06 data.

Figure 3.5 presents the four stable and distinct modes modeled with flat bottom and frequency of 100Hz. The coherence of each individual mode appeared to be very stable over one hour calculated time.

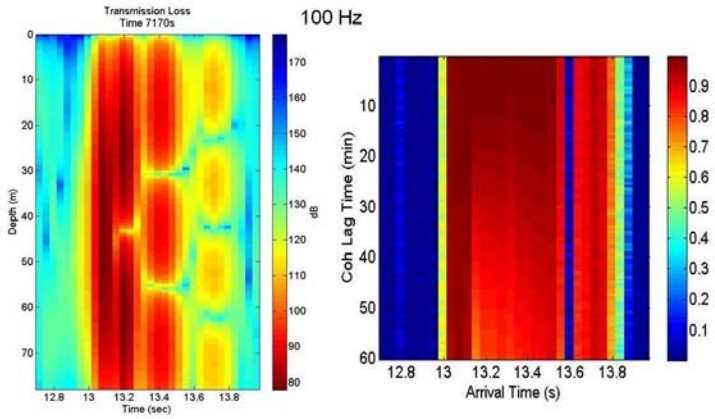

Figure 3.5: 100 Hz modeled data. Flat bottom mode structure (left) and flat bottom temporal coherence (right).

Figures 3.6 and 3.7 show the result for the 400Hz and 800Hz frequencies. As shown in both figures there are very stable modes over the water column, but only the first mode remains coherent and the higher order modes begin to drop off.

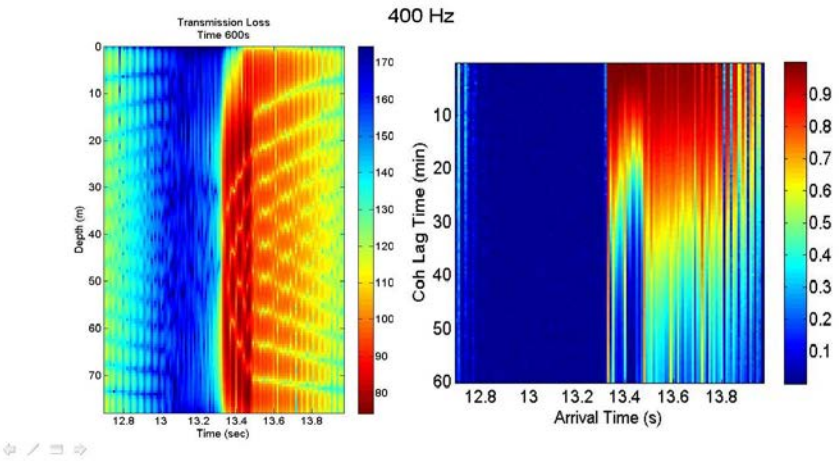

Figure 3.6: 400 Hz modeled data. Flat bottom mode structure (left) and flat bottom temporal coherence (right).

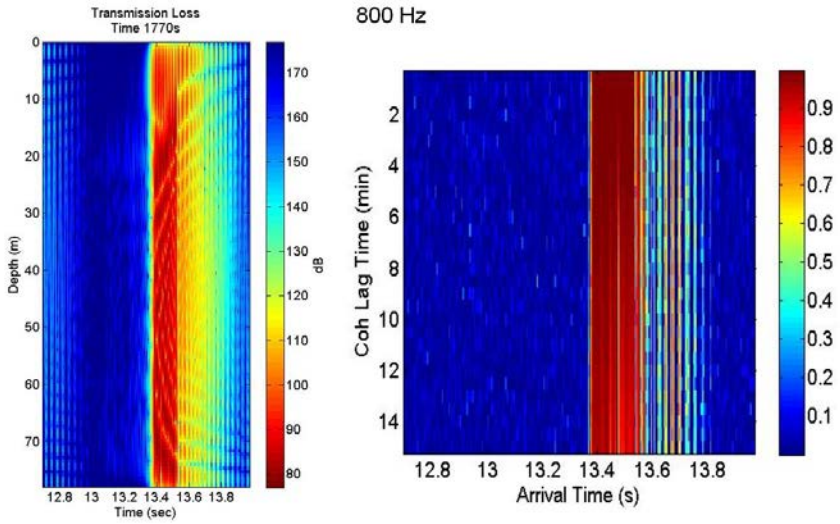

Figure 3.7: 800 Hz modeled data. Flat bottom mode structure (left) and flat bottom temporal coherence (right).

Figures 3.8 and 3.9 show the modeled temporal coherence for two different time frames, the first one with 4 hours of input data and the second one with 8 hours. Both

used 100 Hz as a center frequency. As time progress all modes appear to be affected the same way. This result is in remarkable close agreement with data from the experiment.

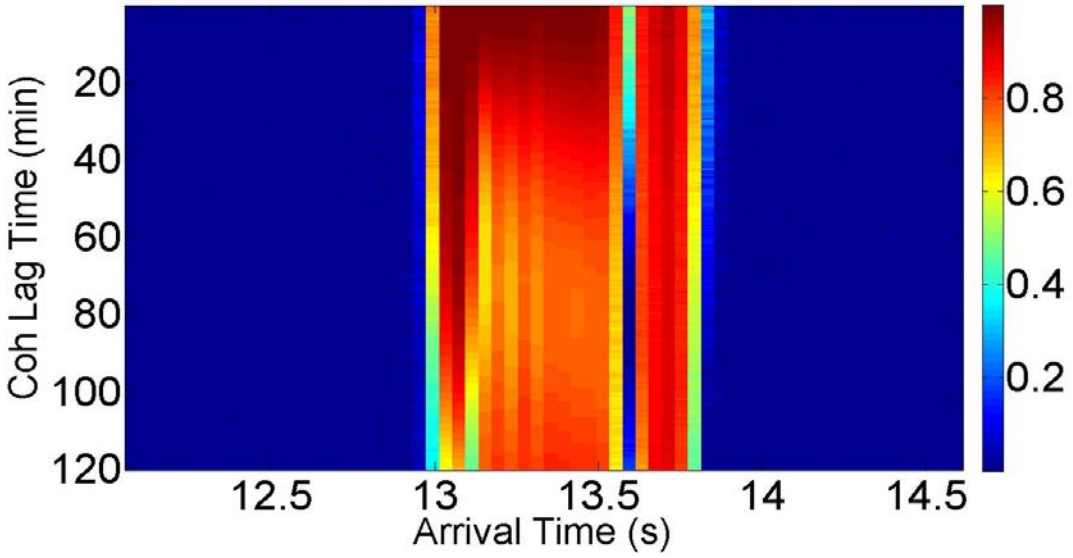

Figure 3.8: 100 Hz modeled temporal coherence for 4 hours of input data.

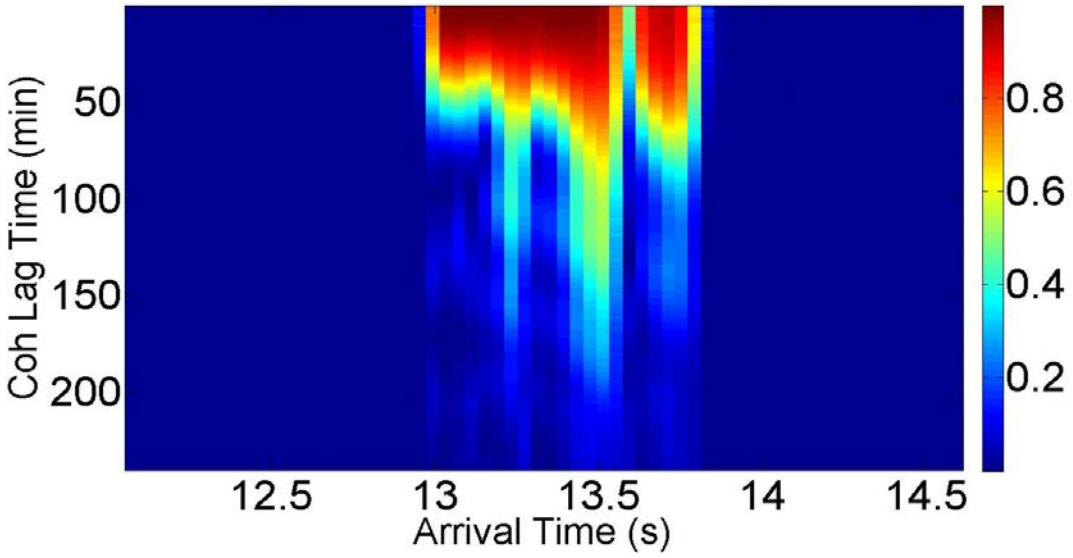

Figure 3.9: 100 Hz modeled temporal coherence for 8 hours of input data.

Similarly, figures 3.10 and 3.11 show the same analysis but this time for 200 Hz as a center frequency. Figure 3.12 shows the modeled temporal coherence for 400 Hz center frequency. The results follow the previous one where it was shown that

lower and higher order modes are affected the same way by the sound speed fluctuations.

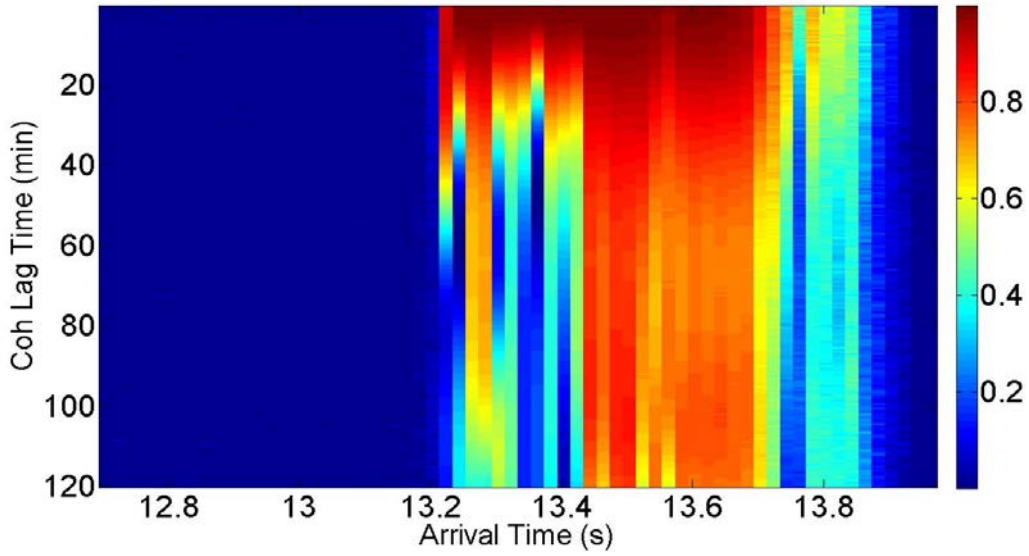

Figure 3.10: 200 Hz modeled temporal coherence for 4 hours of input data.

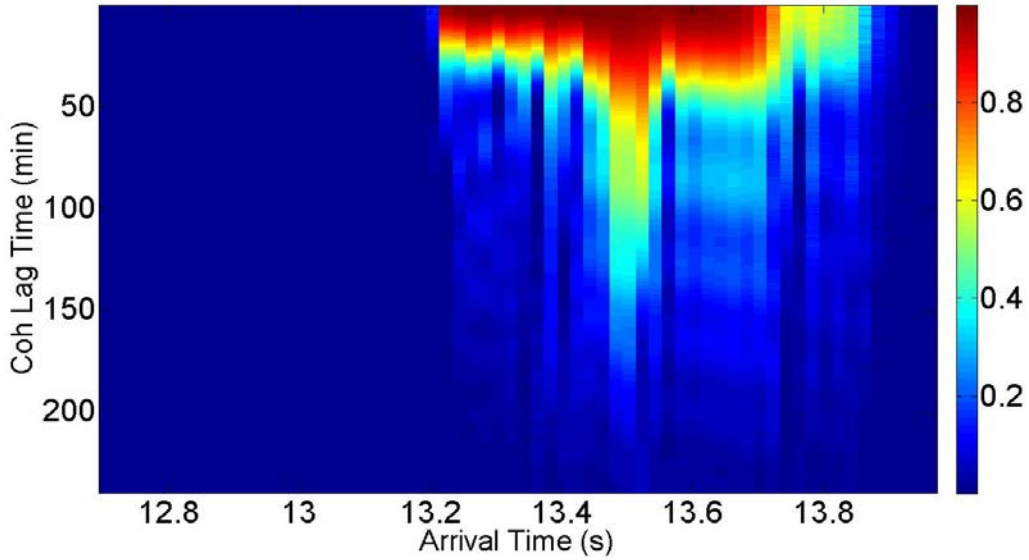

Figure 3.11: 200 Hz modeled temporal coherence for 8 hours of input data.

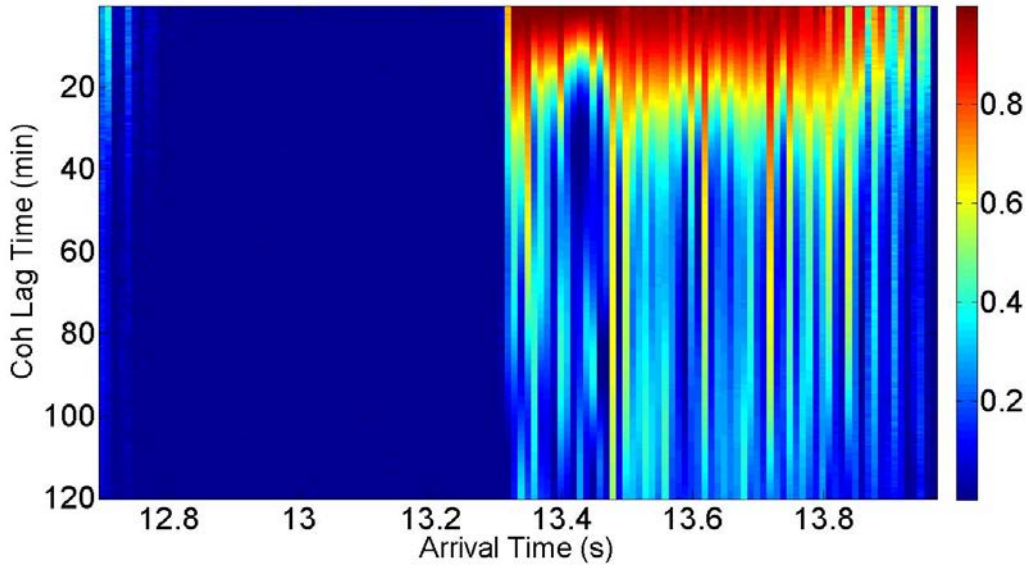

Figure 3.12: 400 Hz modeled temporal coherence for 4 hours of input data.

3.2 RAW DATA AFTER AVERAGING

Another calculation that was made used the full water column SSP after using a 8 hour running average filter on the data. This value was chosen because it kept the internal wave signal while avoiding the background noise. Here on figures 3.13 and 3.14 it is shown the time series of sensors 6, 7, 8, 9 and 10 and the resultant full water column SSP, respectively.

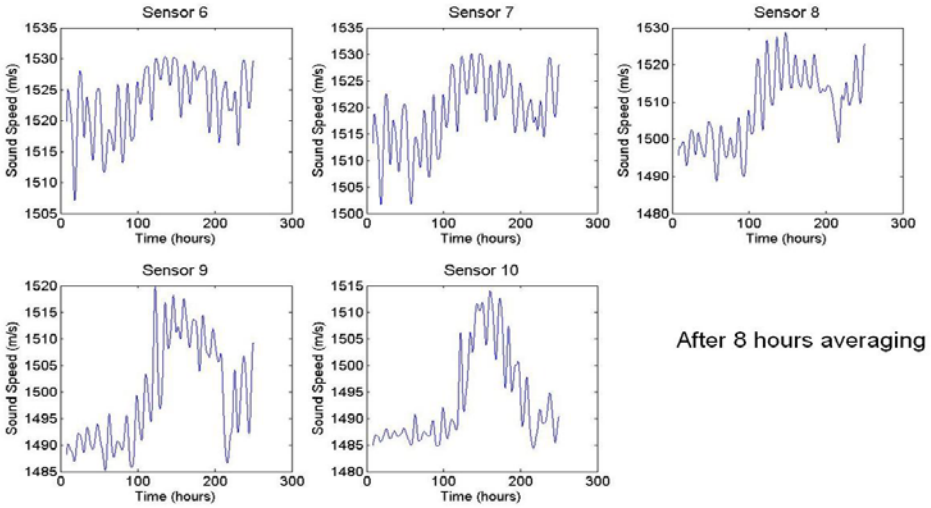

Figure 3.13: Time series of sensors 6, 7, 8, 9 and 10 (Raw data) after 8 hours averaging (running average).

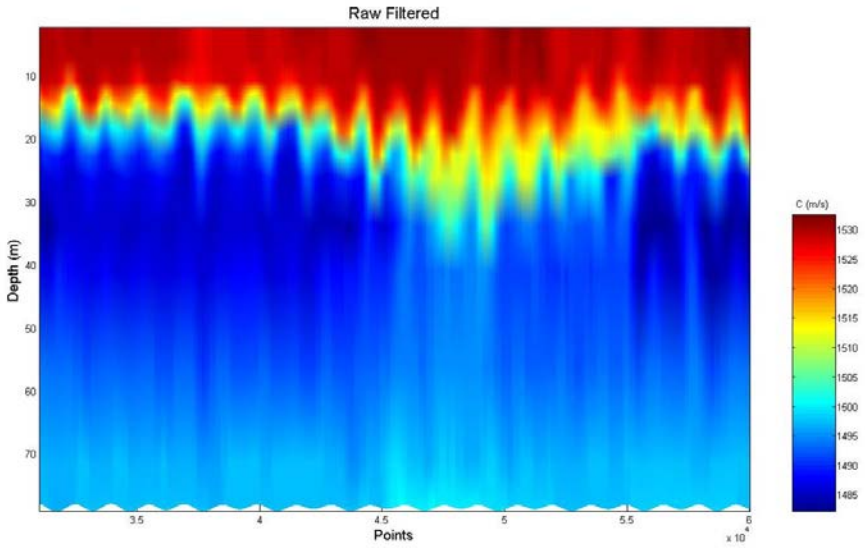

Figure 3.14: Full water column SSP after 8 hours averaging (running average).

3.2.1 RESULTS

The calculation was repeated using the SSP after averaging. The results can be seen in figures 3.15, 3.16 and 3.17 and appear very similar to the previous results.

Nevertheless, we have to keep in mind that we are analyzing only one variable: the fluctuations caused by the passage of an internal wave. There are other variables that contribute to loss of coherence like bottom interactions, source motion among others.

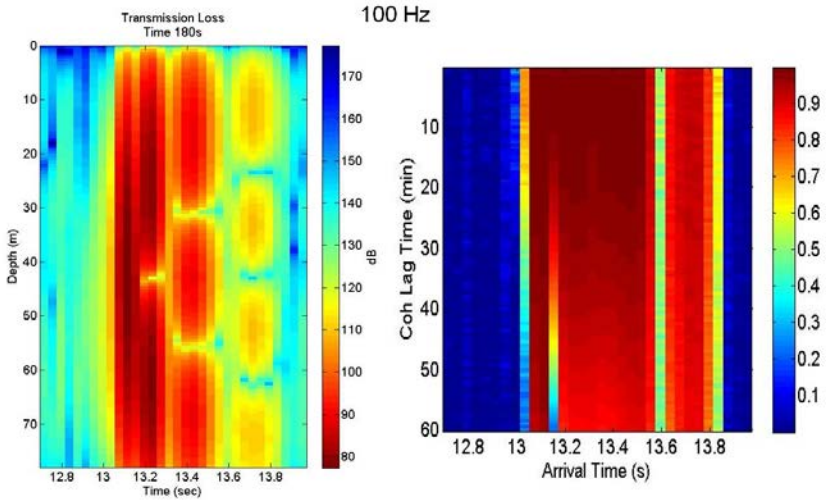

Figure 3.15: 100 Hz modeled data. Flat bottom mode structure (left) and flat bottom temporal coherence (right).

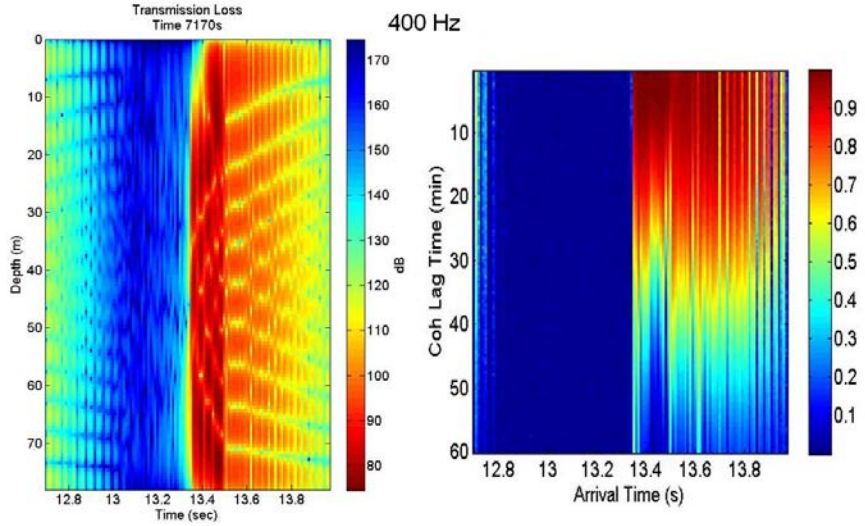

Figure 3.16: 400 Hz modeled data. Flat bottom mode structure (left) and flat bottom temporal coherence (right).

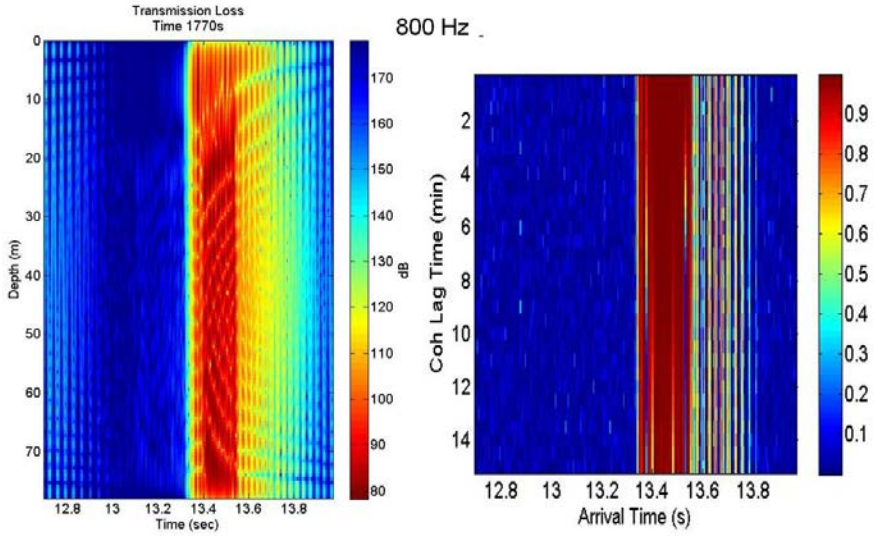

Figure 3.17: 800 Hz modeled data. Flat bottom mode structure (left) and flat bottom temporal coherence (right).

3.3 THE BACKGROUND INTERNAL WAVE FIELD

So far an ideal model regarding the internal wave setup has been used, as range dependence of the IW wasn't taken into account. In the following section the contribution of range dependence on the coherence will be investigated. Figure 3.8 presents the moorings that will be used for this modeling.

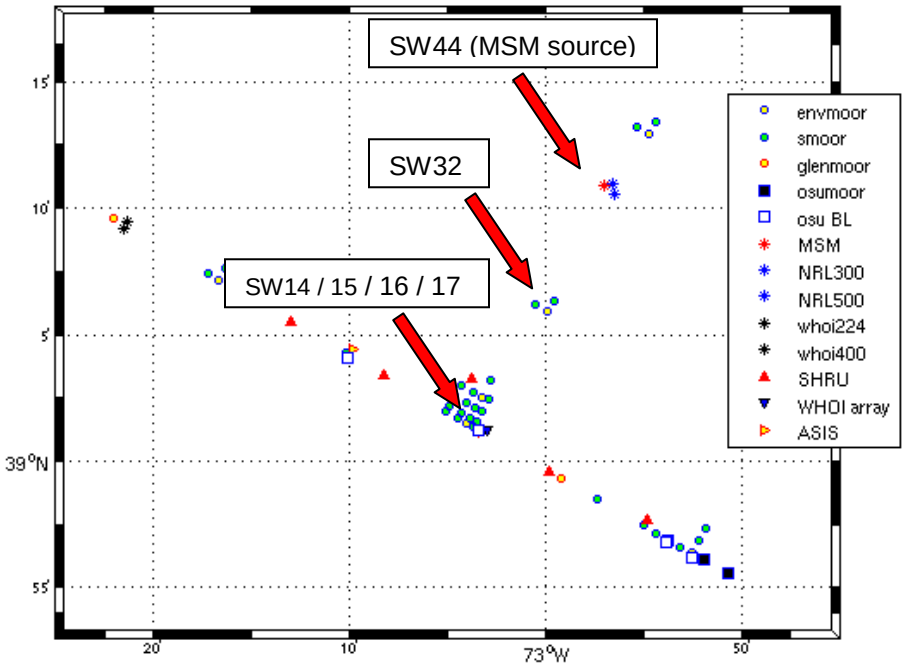

Figure 3.18: SW06 Chart with moorings and locations. Reprinted from Woods Hole Oceanog. Inst. Tech. rept., WHOI-2007-04.

The distance in nautical miles between moorings is presented in the following table:

Moorings	**SW14**	**SW15**	**SW16**	**SW17**	**SW32**	**SW44 (MSM)**
SW 14	-	0.6 Mi	1.4 Mi	2.4 Mi	6.2 Mi	11.5 Mi
SW 15	0.6 Mi	-	0.8 Mi	1.8 Mi	5.6 Mi	
SW 16	1.4 Mi	0.8 Mi	-	1.0 Mi	4.8 Mi	
SW 17	2.4 Mi	1.8 Mi	1.0 Mi	-	3.8 Mi	9.1 Mi
SW 32	6.2 Mi	5.6 Mi	4.8 Mi	3.8 Mi	-	5.3 Mi
SW44 (MSM)	11.5 Mi	10.9 Mi	10.1 Mi	9.1 Mi	5.3 Mi	-

Table 3.1: Distance in nautical miles between moorings showed in Figure 3.13

For the horizontal coherence calculation we are going to use the following thermistors:

Moorings	**Thermistor's Depth**
SW 14	25 m
SW 15	25 m
SW 16	25 m
SW 17	25 m
SW 32	21 m
SW44 (MSM)	75 m

Table 3.2: Depth of thermistors used in the horizontal coherence calculation

It is going to be shown later that almost all sound speed fluctuations occur at mid-depths. Thus, we tried to make the horizontal coherence calculation using sensors as close as possible to the mid-depth water column. At the source, i.e. Mooring SW44, there wasn't a mid-depth sensor so the one at 75 m was chosen since the other one was located at the surface.

3.3.1 Horizontal Coherence

Matlab was used to perform the horizontal coherence calculation. The time series were demeaned and a cosine bell filter using 60 Fourier coefficients was used to calculate the cross-spectra between moorings. The results can be seen in figures 3.19, 3.20, 3.21 and 3.22.

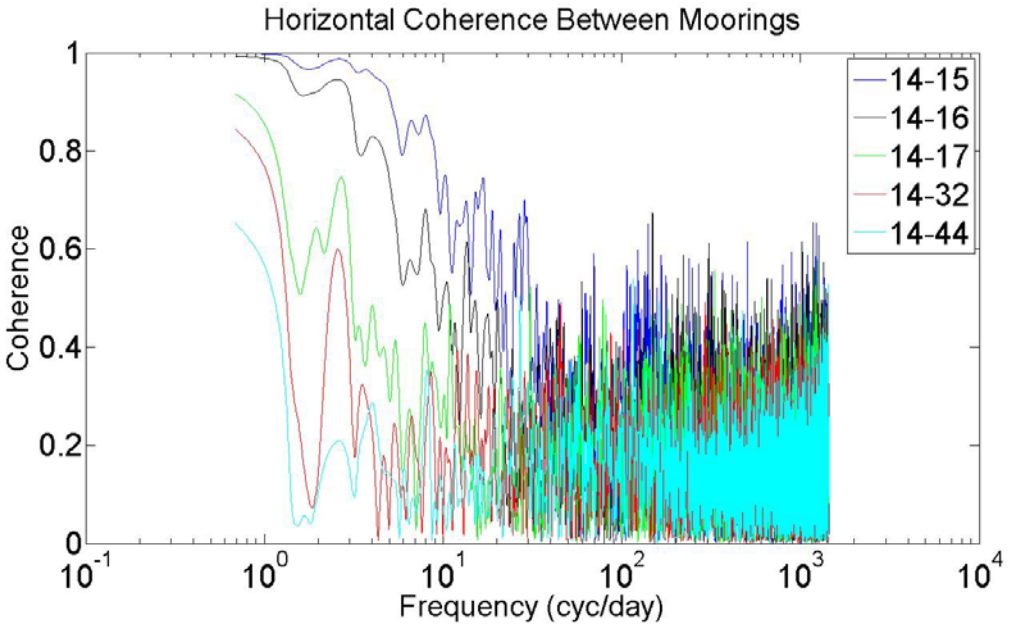

Figure 3.19: Figure shows the horizontal coherence between mooring 14 and the other ones in sequence.

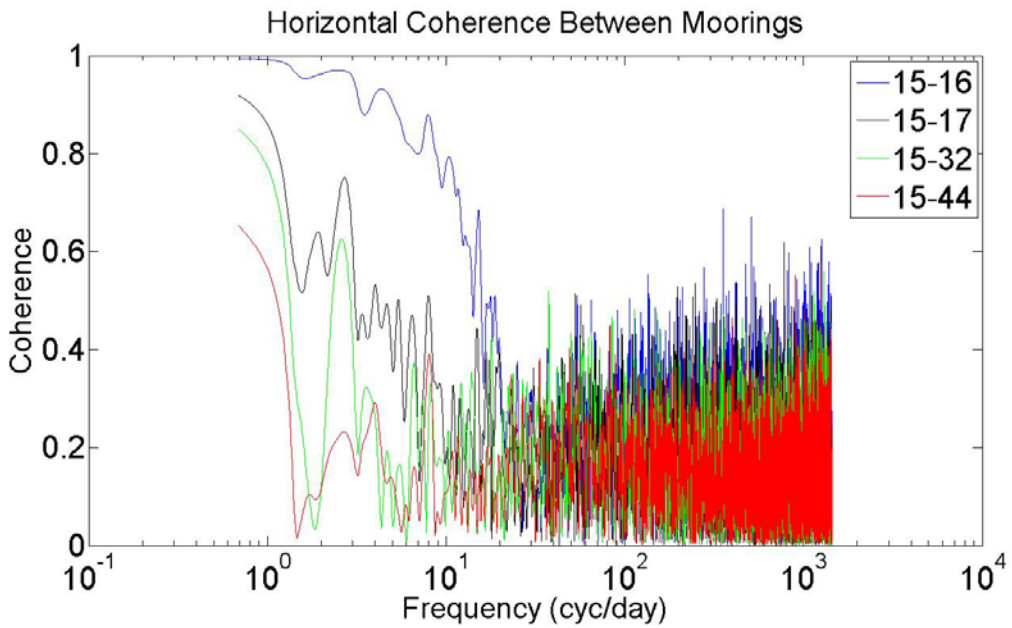

Figure 3.20: Figure shows the horizontal coherence between mooring 15 and the other ones in sequence.

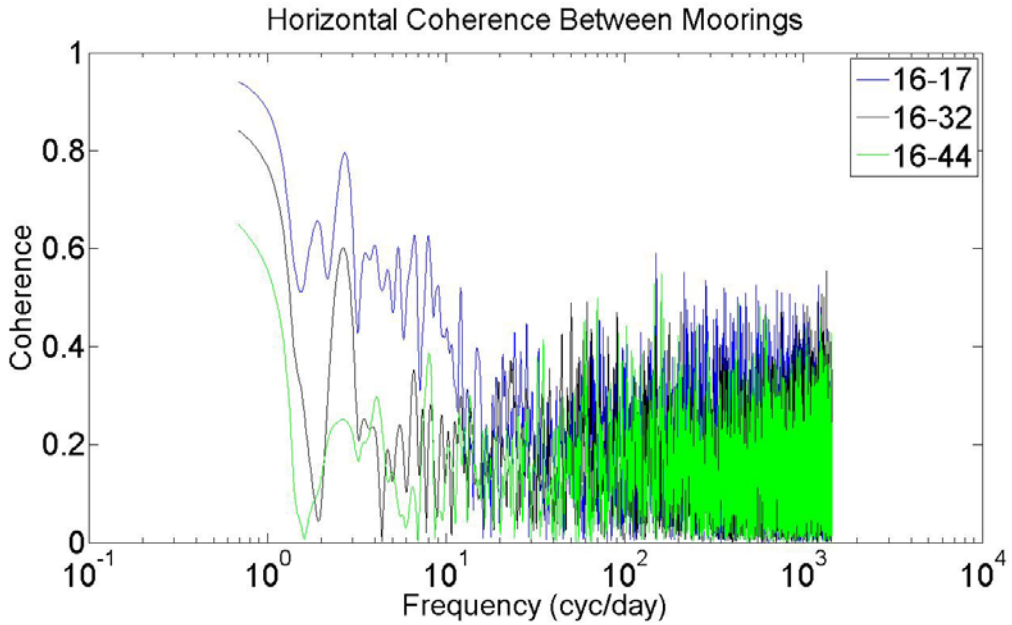

Figure 3.21: Figure shows the horizontal coherence between mooring 16 and the other ones in sequence.

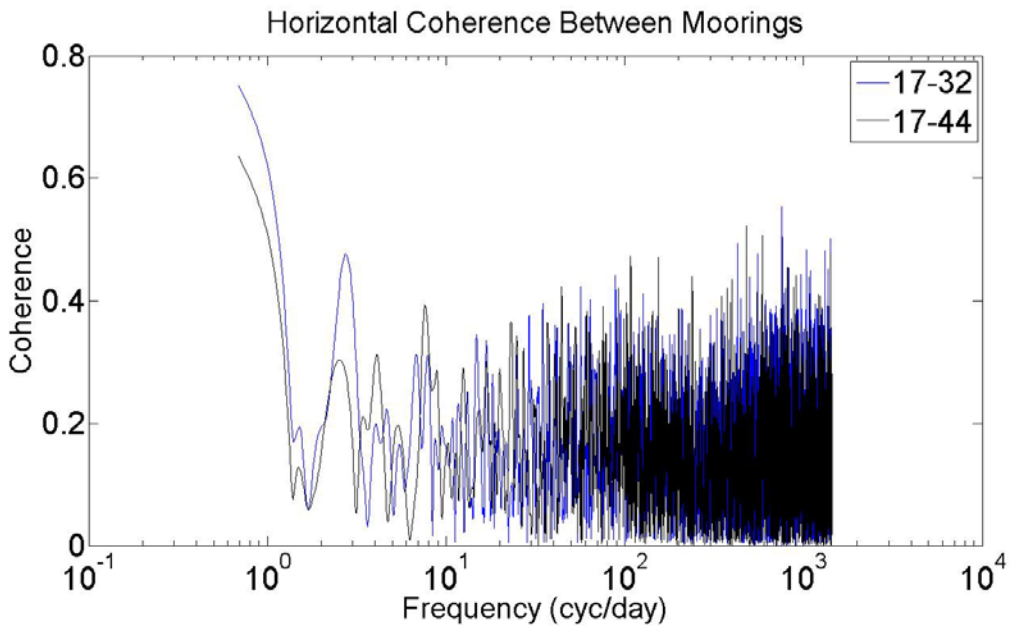

Figure 3.22: Figure shows the horizontal coherence between mooring 17 and the other ones in sequence.

As shown in figures 3.19, 3.20, 3.21 and 3.22 that the lower band of the spectra has a general decreasing coherence as a function of range but a very good agreement in phase. Moving up in spectra the phase coherence is lost and the coherence is a randomized value even for close moorings.

3.3.2 VERTICAL COHERENCE

In this section an analysis of the vertical coherence between the sensors deployed at the Shark array location will be performed. Fifteen sensors and 30000 samples, equivalent to 250 hours of data collection, were used. The mean depth for each sensor can be found in Table 3.3.

Sensor	Mean depth (m)
1	2.46
2	4.47
3	6.48
4	7.48
5	10.96
6	13.21
7	15.01
8	18.76
9	22.51
10	26.26
11	33.76
12	41.26
13	56.26
14	71.26
15	78.46

Table 3.3: Mean depth of sensors

A Matlab routine was used to calculate the vertical coherence between all sensors. Sensor 9 was used as a basis to all plots since at this depth we can find the highest amplitude averages as shown in figure 3.23.

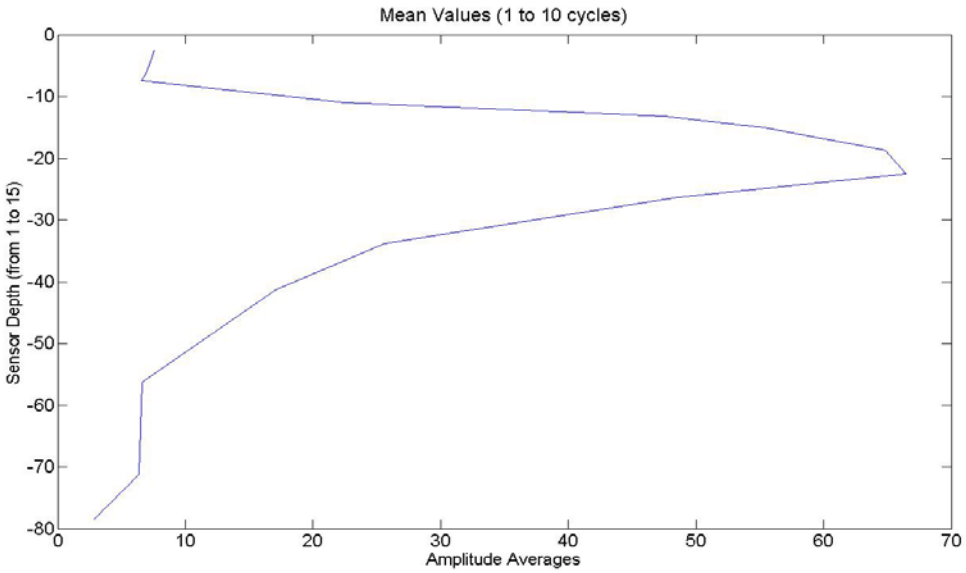

Figure 3.23: Figure shows the mean amplitude averages for a 1 to 10 cycles per day band of frequencies.

As shown in previous sections, the time series were demeaned and a cosine bell filter using 120 Fourier coefficients was used to calculate the cross-spectra between moorings. The results can be seen in figures 3.24, 3.25, 3.26 and 3.27. It is shown that between mid-depth sensors the coherence is most stable and the phase oscillation is nearly constant. However the same stability is not present between sensor 9 and the more bottom or surface located sensors. The coherence starts to increase between mid-depth sensors until a value of about 0.65. This occurs between a band of frequencies of 150 and 290 cycles per day. The tidal periodicity of the internal wave train occurrence was found to be 5-9 minutes and the heights from 10-15 m, up to 25 m (Serebryany et al 2008). This periodicity corresponds to 160-288 cycles per day. As a consequence, it is hypothesized that the increase in coherence is due to the passage of the internal wave train.

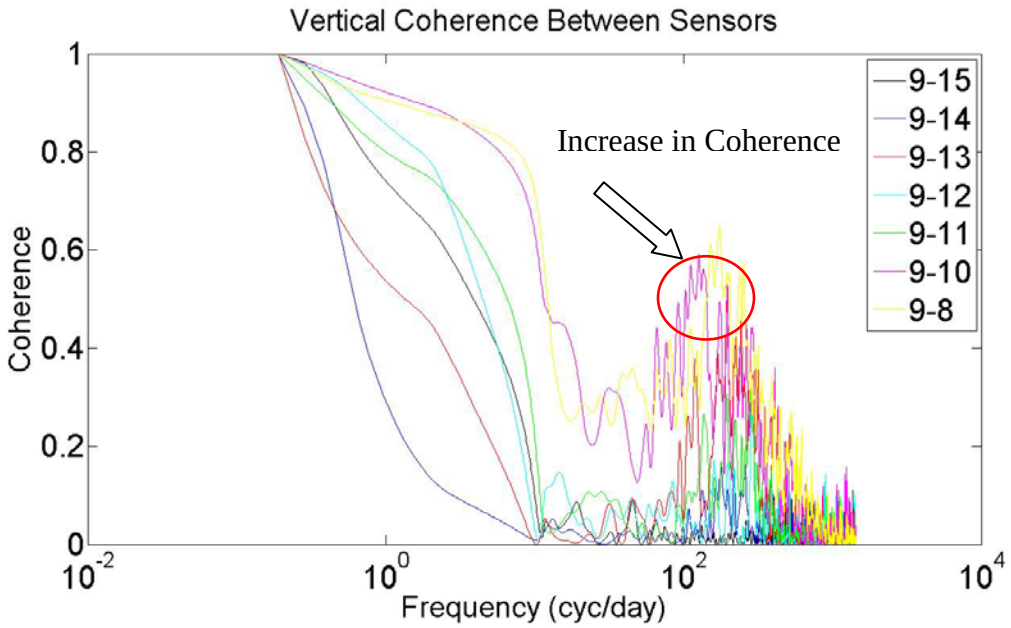

Figure 3.24: Figure shows the vertical coherence between sensor 9 and the other ones in sequence.

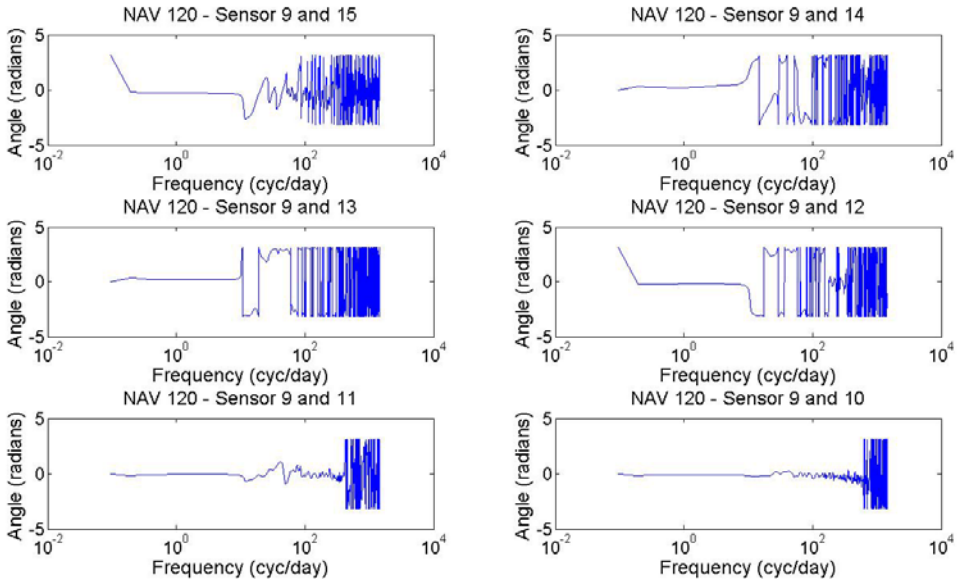

Figure 3.25: Figure shows the phase oscillation between sensor 9 and the other ones in sequence.

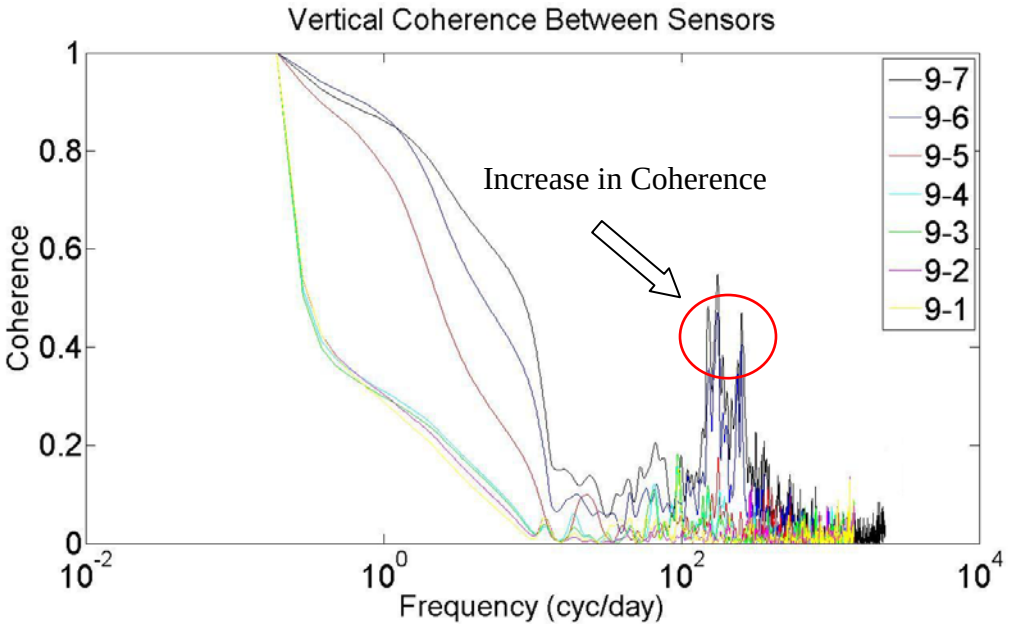

Figure 3.26: Figure shows the vertical coherence between sensor 9 and the other ones in sequence.

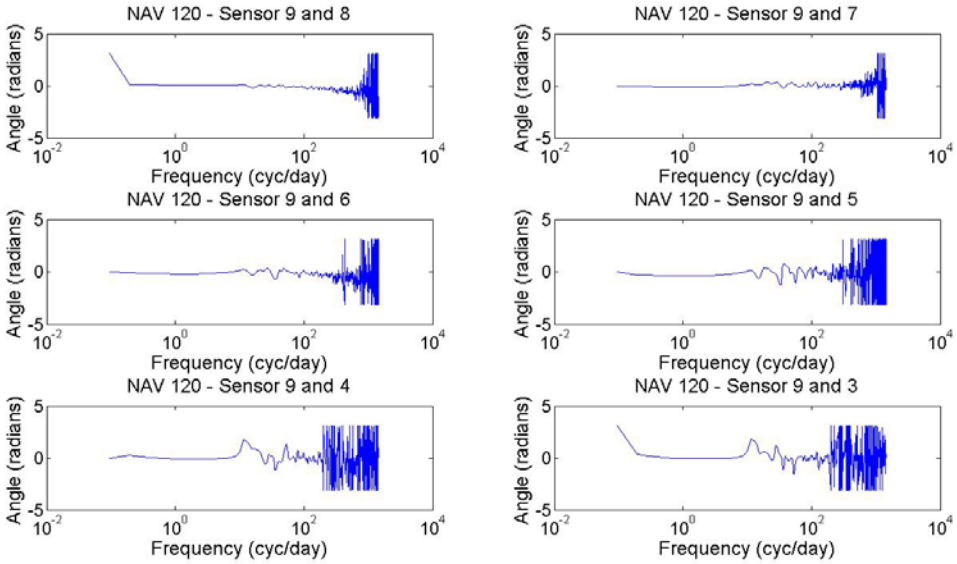

Figure 3.27: Figure shows the phase oscillation between sensor 9 and the other ones in sequence.

3.3.3 BANDS AND MEAN VALUES

This section will show how different bands of frequency contribute to the general sound speed profile. To do that, the spectrum was divided in several bands (10 cycles band) and the amplitude average was computed for every band. The result can be seen in figure 3.28. The highest value occurs almost always at the same sensor, i.e., sensor 9 which corresponds to 22 m depth, the same depth in which there is the strongest sound speed variation due to the passage of the train of solitons. Also importantly, the lower frequency bands have a bigger contribution than higher ones. The amplitude averages are nearly constant near the bottom and surface and between about 10 and 26 m depth higher oscillations are observed. This difference of about 16 m happens to be of the same order of the internal wave heights (from 10-15 m, up to 25 m) found by Serebryany et al 2008.

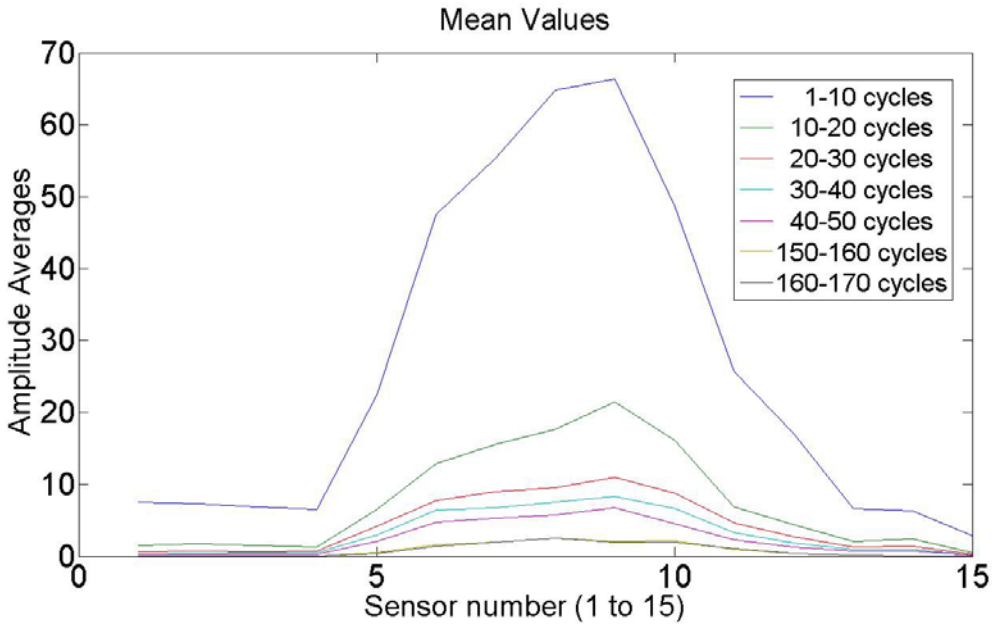

Figure 3.28: Figure shows the vertical coherence between sensor 9 and the other ones in sequence.

3.4 MODEL PREDICTIONS FOR ACOUSTIC MODE COHERENCE

In this section the effect of frequency filters on the acoustic mode coherence will be shown, with data from the Shark mooring used as input. As mentioned in previous sections, the data were demeaned and filtered using different frequencies as a basis for our experiment and time series from a thermistor located at mid-depth (41m) was used.

3.4.1 RESULTS FOR DIFFERENT FILTERS

Figure 3.29 shows mode coherence using six different filters. The upper part has the power spectral density of the thermistor at 41m depth and the lower part shows six coherence panels for different frequencies as labeled. The center frequency used was 100Hz for all panels. Panels one, two and three have very coherent modes for 30 minutes of coherence calculation. Beginning in panel four, it is shown that the higher order modes

start to break up as the first mode remains stable. At higher frequencies, in this case 160 and 288 cycles per day, the first mode begins to break up. These frequencies correspond to the tidal periodicity of internal wave train occurrence (Serebryany et al 2008).

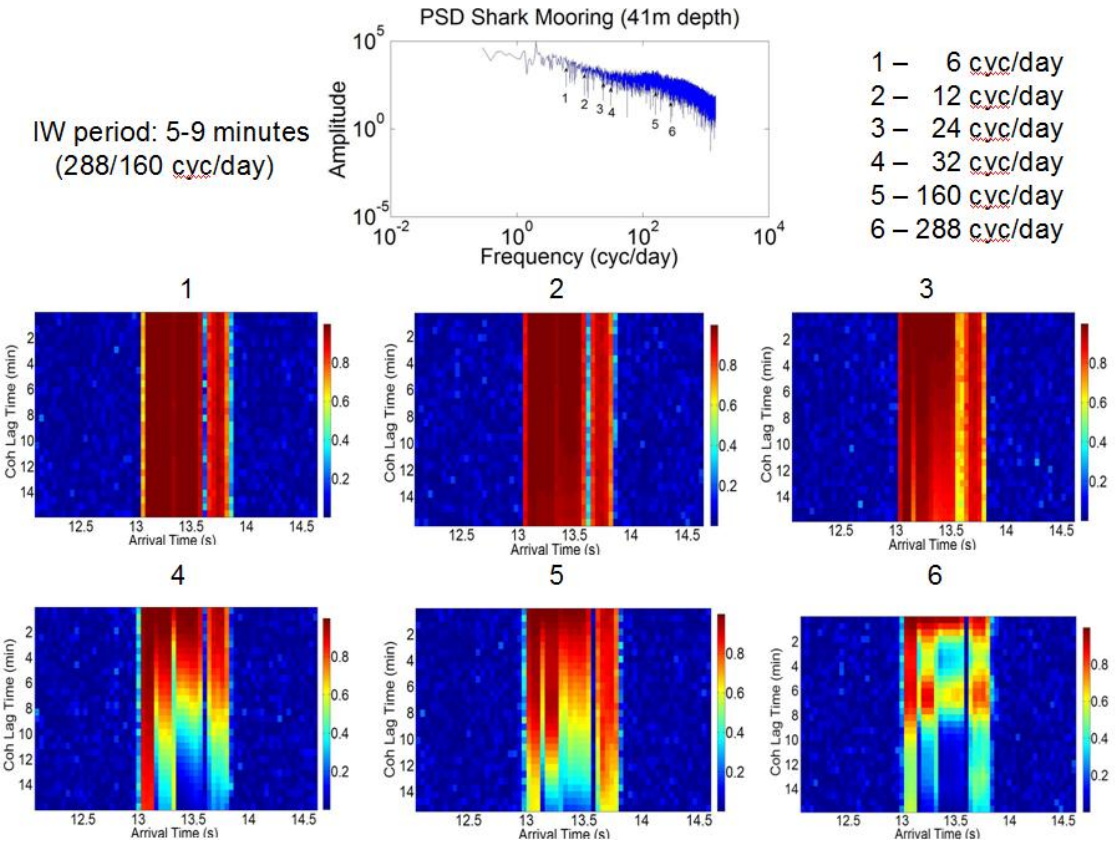

Figure 3.29: Figure shows the mode coherence using 6 different frequencies.

Based on the results found in figure 3.29, it was decided to assay the data from the Shark array using 5 different bands of frequency. Figure 3.30 shows how the bands were determined.

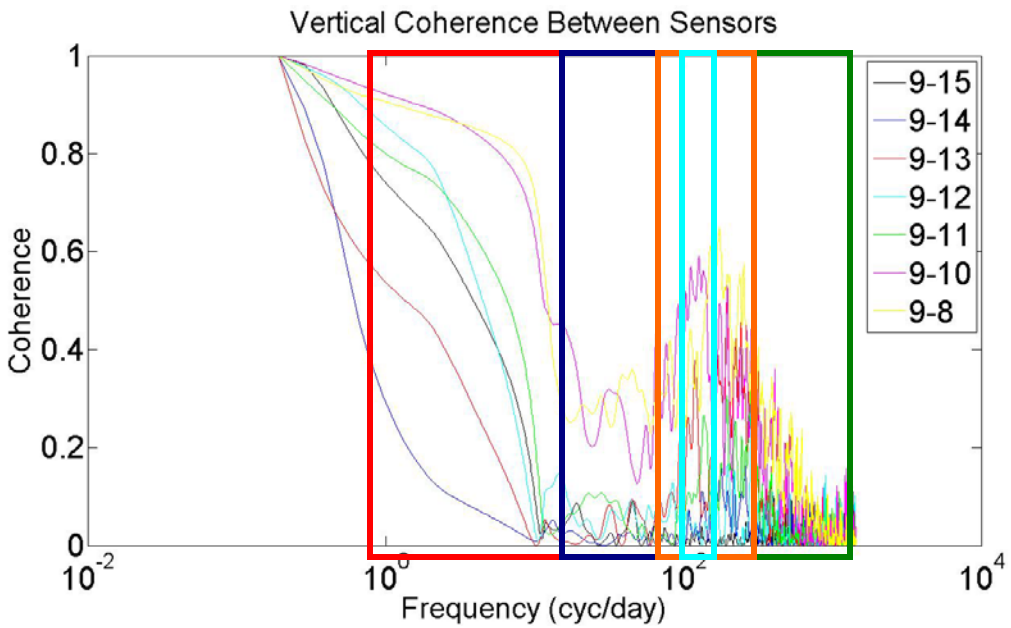

Figure 3.30: Figure shows vertical coherence between sensors and bands.

The first band boxed in red represents the lower part of the spectrum where the coherence has higher values and is phase coherent. The second band in dark blue has low coherence values. The third band in orange has coherence values of almost 0.6 between mid-depth sensors and also a lot of noise and the forth band in dark green is a noisy band in the upper part of the spectrum. The last band in light blue is a very narrow band centered in 160 cycles per day (SIW period).

3.4.2 RESULTS FOR DIFFERENT FREQUENCY BANDS

Figures 3.31, 3.32, 3.33 and 3.34 show the result for the first band at different center frequencies (100Hz, 200Hz, 400Hz and 800Hz).

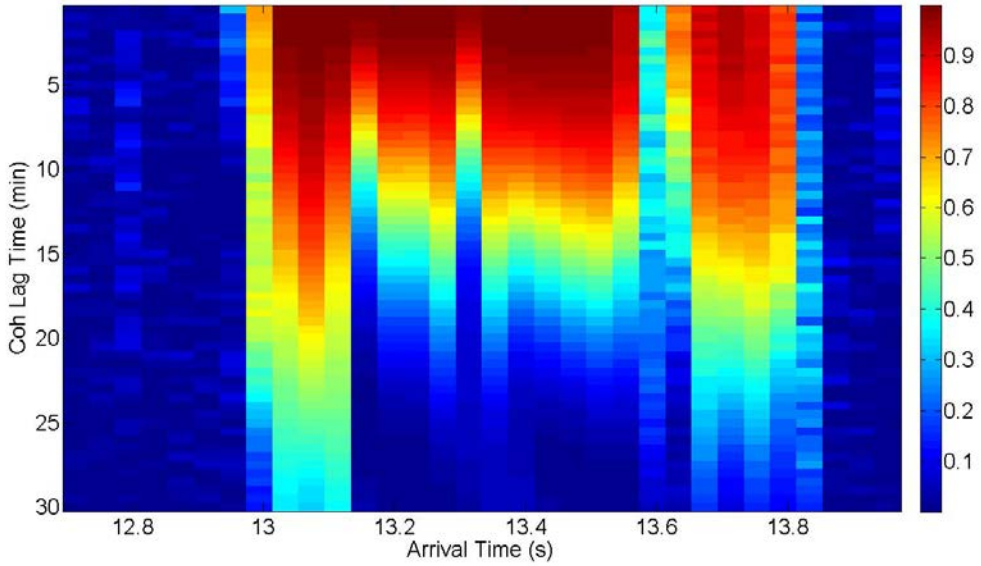

Figure 3.31: Figure shows coherence for the 1st band and center frequency 100 Hz.

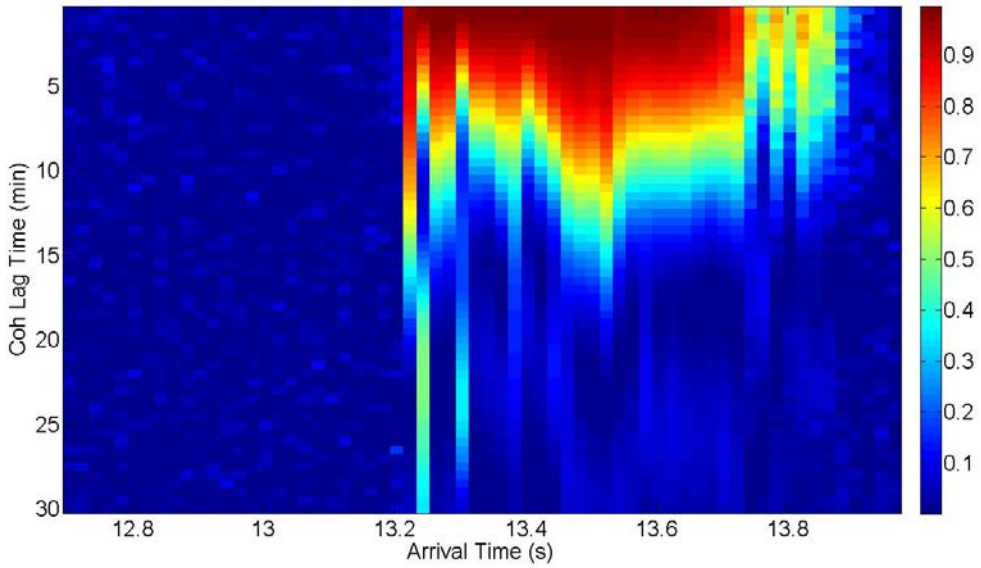

Figure 3.32: Figure shows coherence for the 1st band and center frequency 200 Hz.

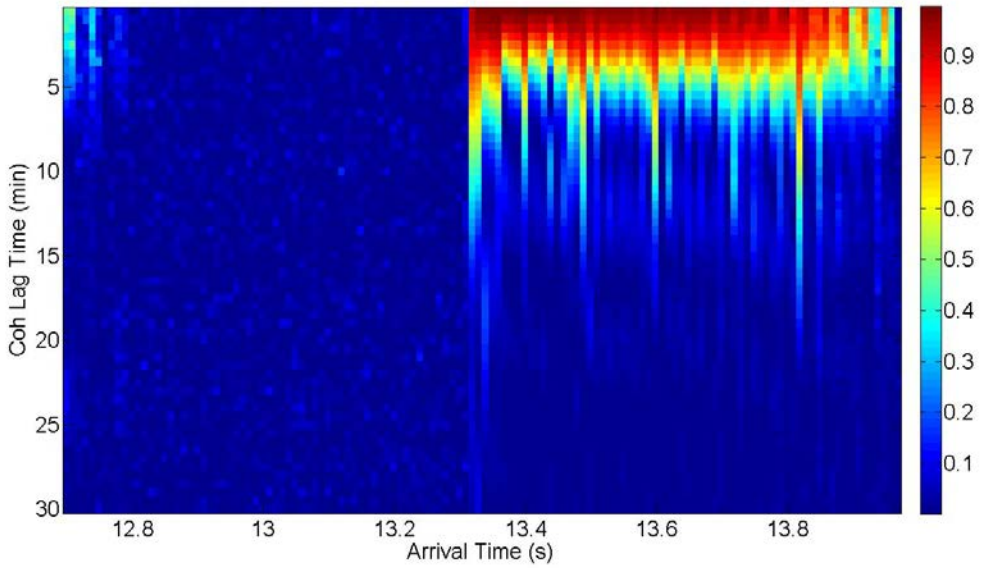

Figure 3.33: Figure shows coherence for the 1st band and center frequency 400 Hz.

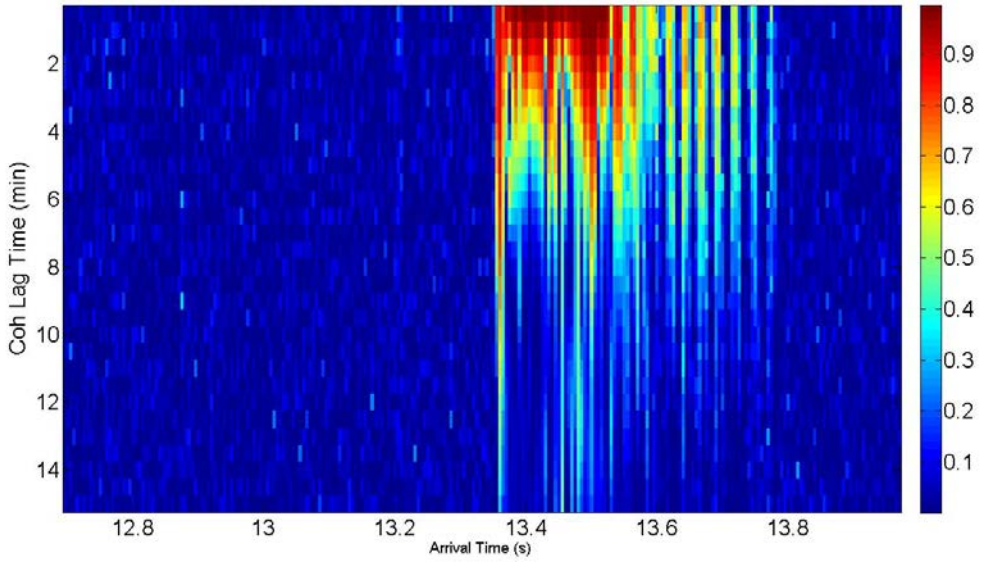

Figure 3.34: Figure shows coherence for the 1st band and center frequency 800 Hz.

Figures 3.35, 3.36, 3.37 and 3.38 show the result for the second band at different center frequencies (100Hz, 200Hz, 400Hz and 800Hz).

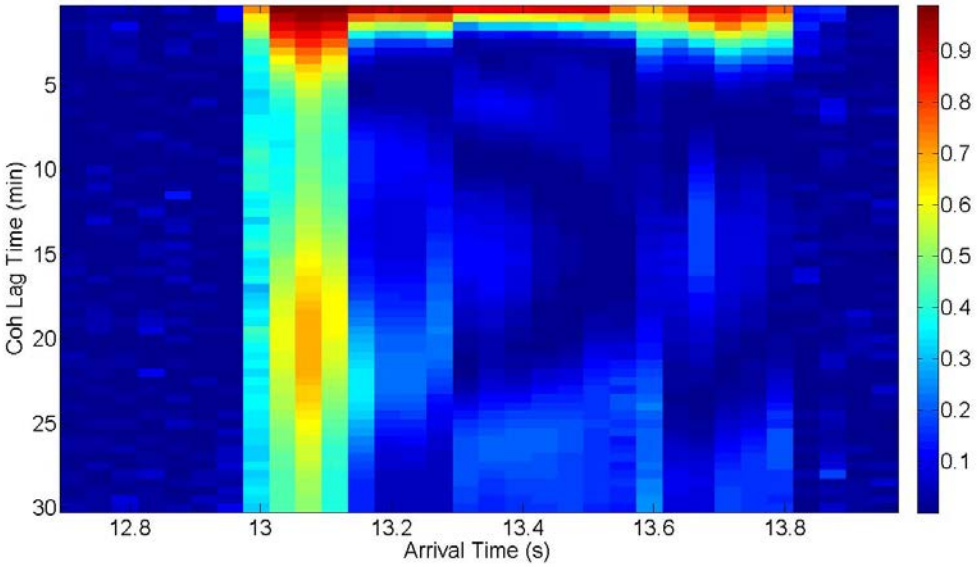

Figure 3.35: Figure shows coherence for the 2nd band and center frequency 100 Hz.

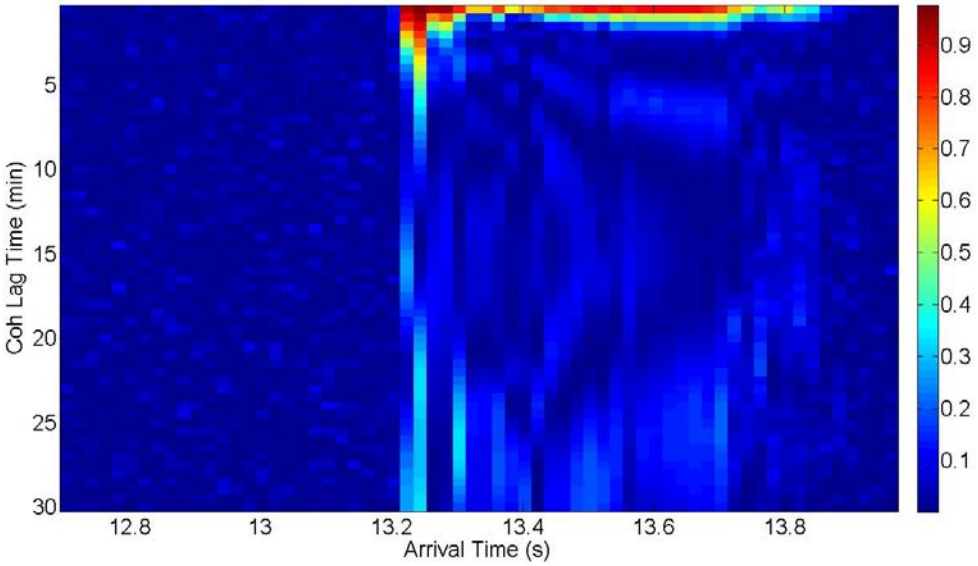

Figure 3.36: Figure shows coherence for the 2nd band and center frequency 200 Hz.

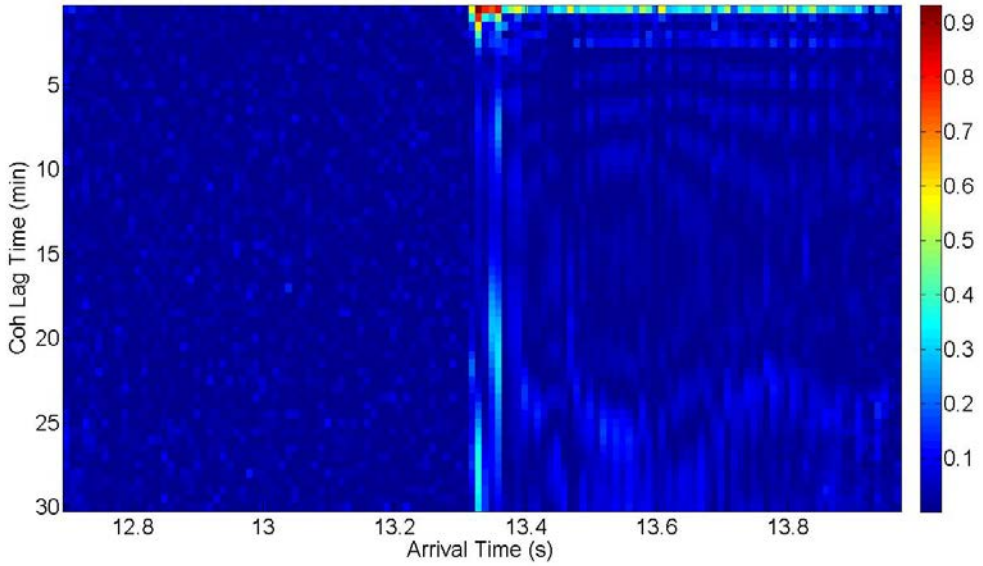

Figure 3.37: Figure shows coherence for the 2nd band and center frequency 400 Hz.

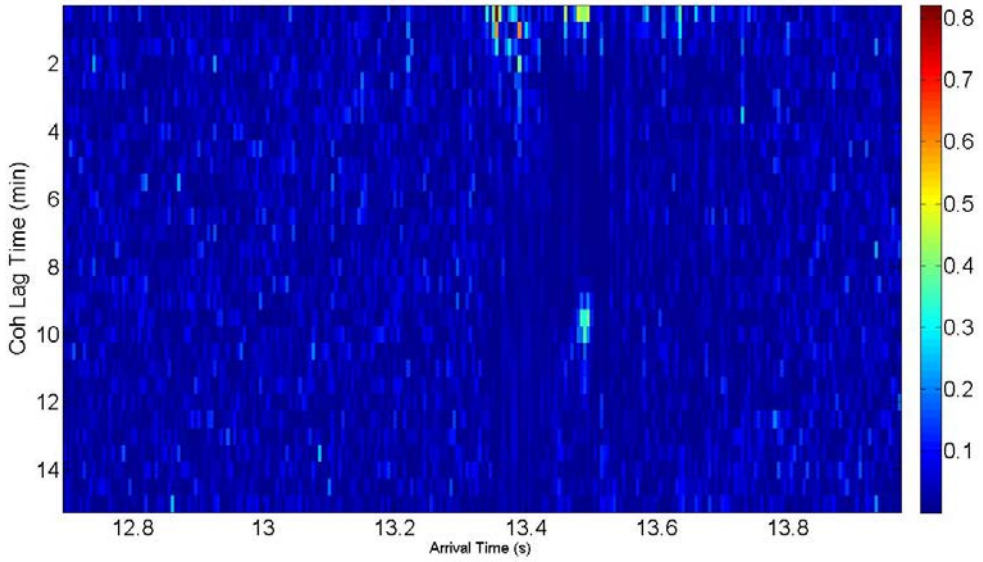

Figure 3.38: Figure shows coherence for the 2nd band and center frequency 800 Hz.

Figures 3.39, 3.40, 3.41 and 3.42 show the result for the third band at different center frequencies (100Hz, 200Hz, 400Hz and 800Hz).

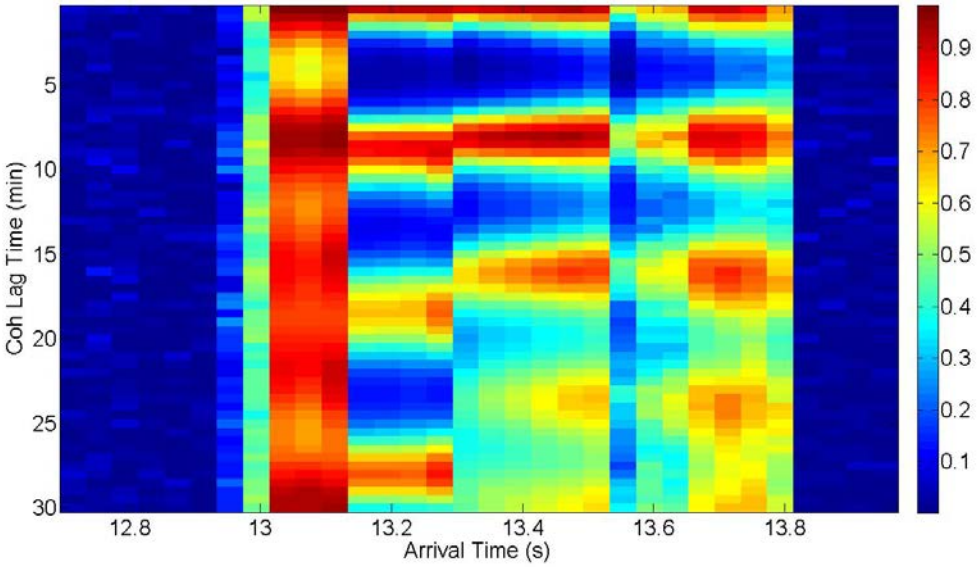

Figure 3.39: Figure shows coherence for the 3rd band and center frequency 100 Hz.

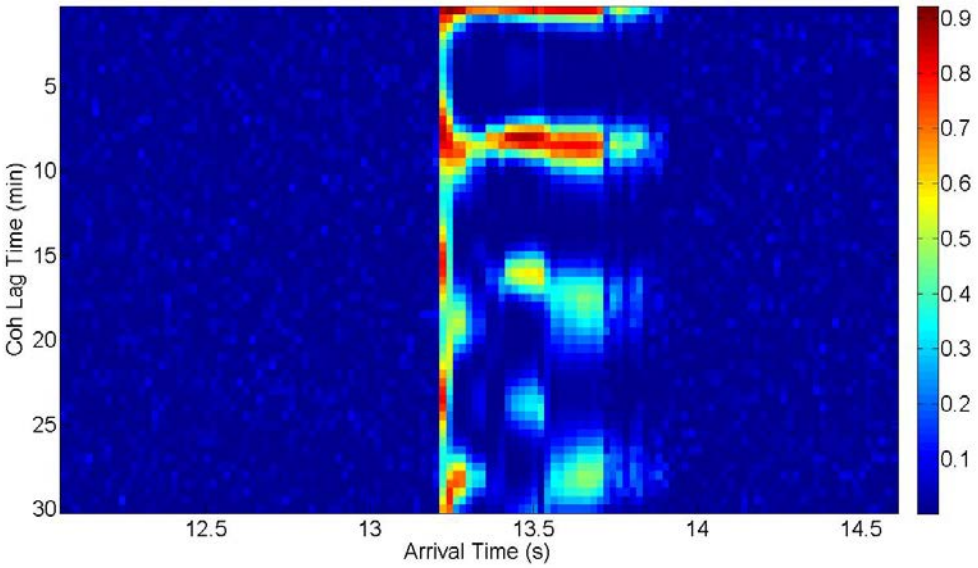

Figure 3.40: Figure shows coherence for the 3rd band and center frequency 200 Hz.

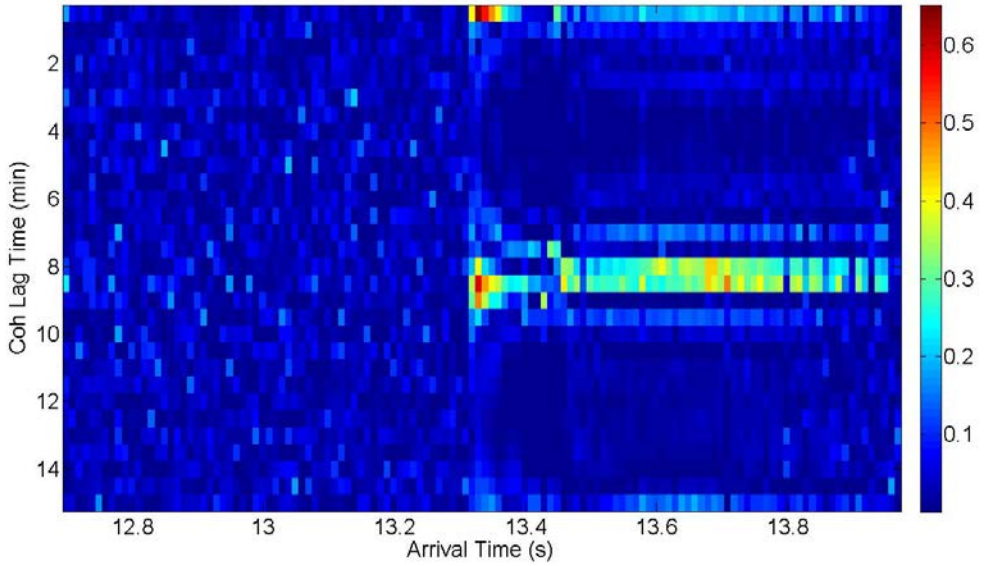

Figure 3.41: Figure shows coherence for the 3rd band and center frequency 400 Hz.

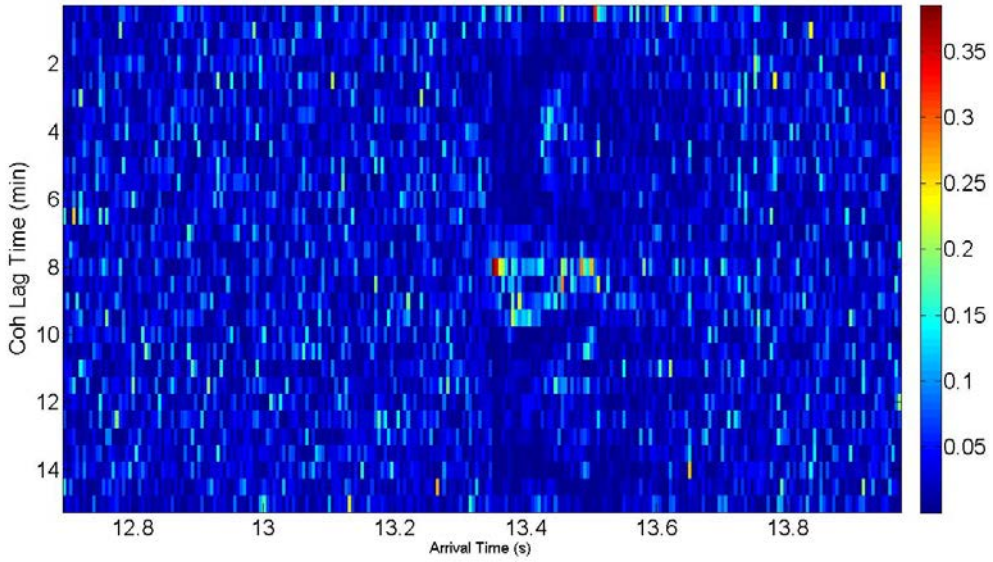

Figure 3.42: Figure shows coherence for the 3rd band and center frequency 800 Hz.

Figures 3.43, 3.44, 3.45 and 3.46 show the result for the forth band at different center frequencies (100Hz, 200Hz, 400Hz and 800Hz).

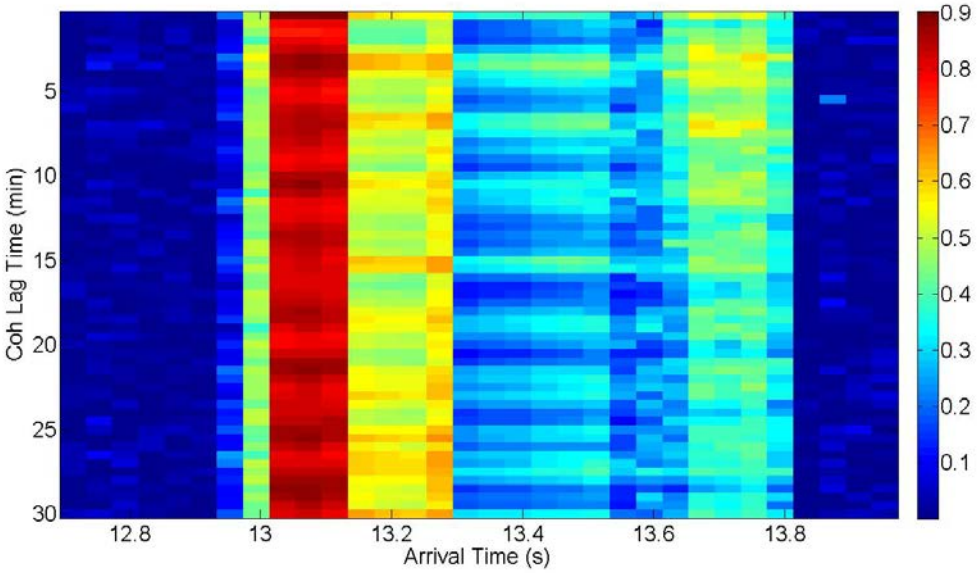

Figure 3.43: Figure shows coherence for the 4th band and center frequency 100 Hz.

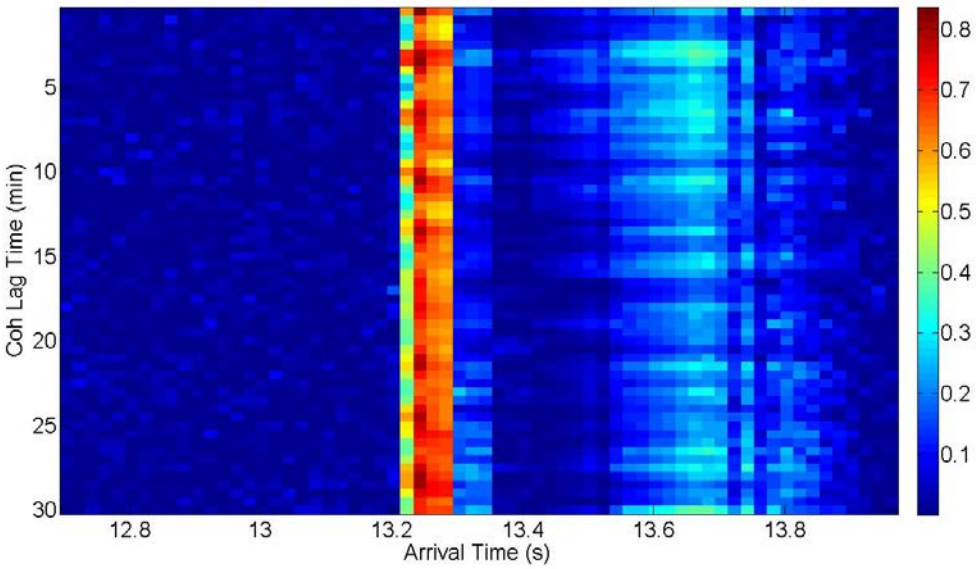

Figure 3.44: Figure shows coherence for the 4th band and center frequency 200 Hz.

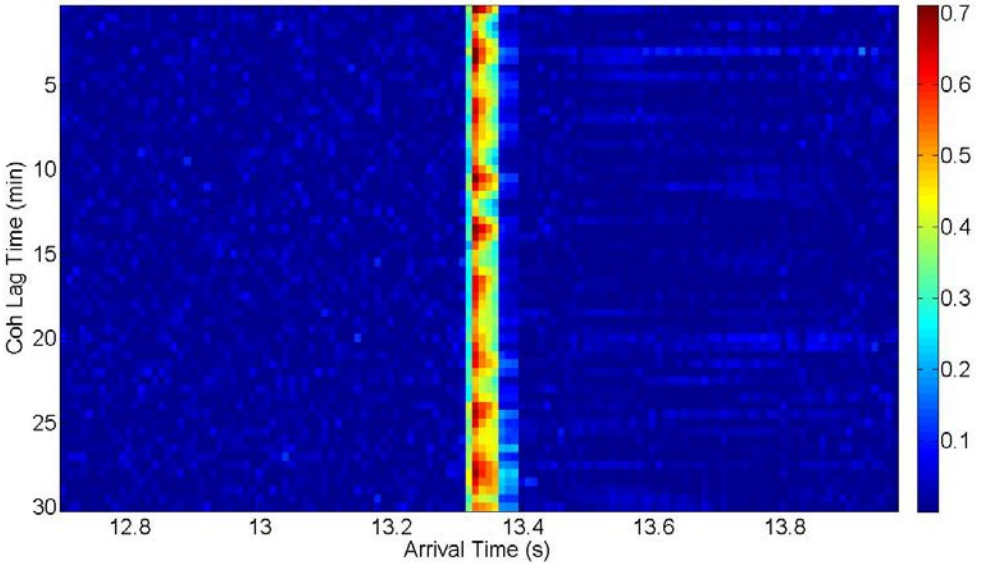

Figure 3.45: Figure shows coherence for the 4th band and center frequency 400 Hz.

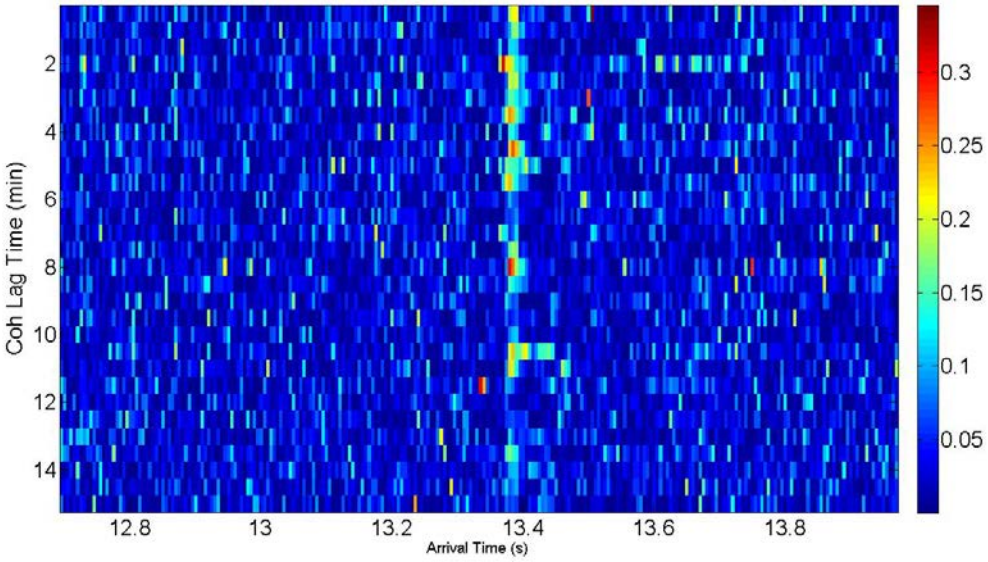

Figure 3.46: Figure shows coherence for the 4th band and center frequency 800 Hz.

Figures 3.47, 3.48, 3.49 and 3.50 show the result for the fifth band at different center frequencies (100Hz, 200Hz, 400Hz and 800Hz).

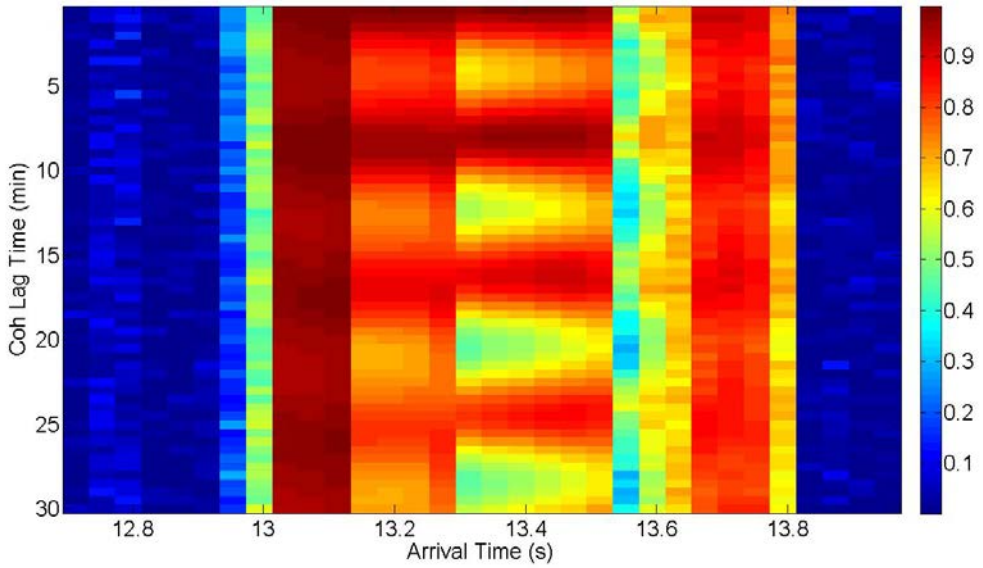

Figure 3.47: Figure shows coherence for the SIW band and center frequency 100 Hz.

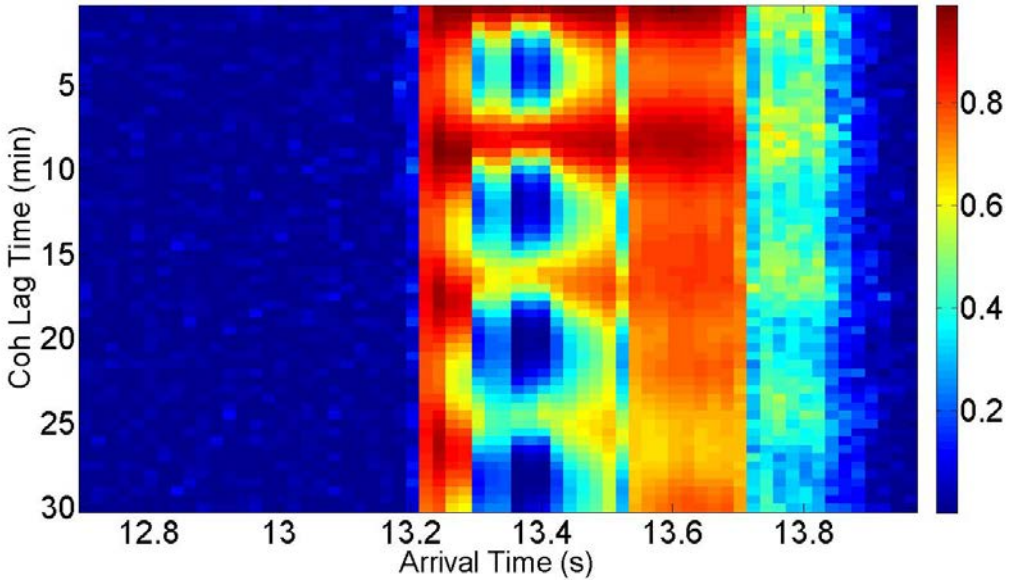

Figure 3.48: Figure shows coherence for the SIW band and center frequency 200 Hz.

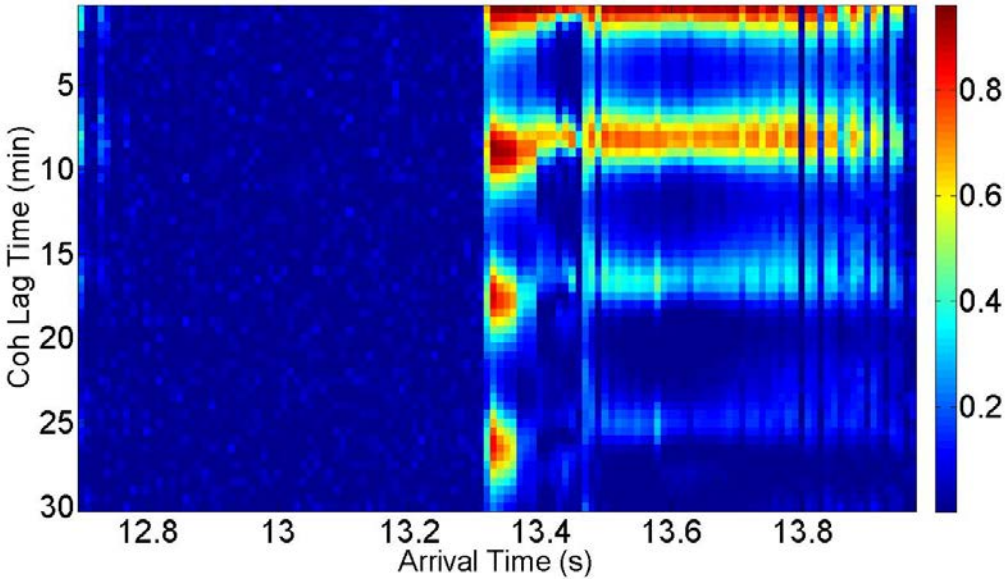

Figure 3.49: Figure shows coherence for the SIW band and center frequency 400 Hz.

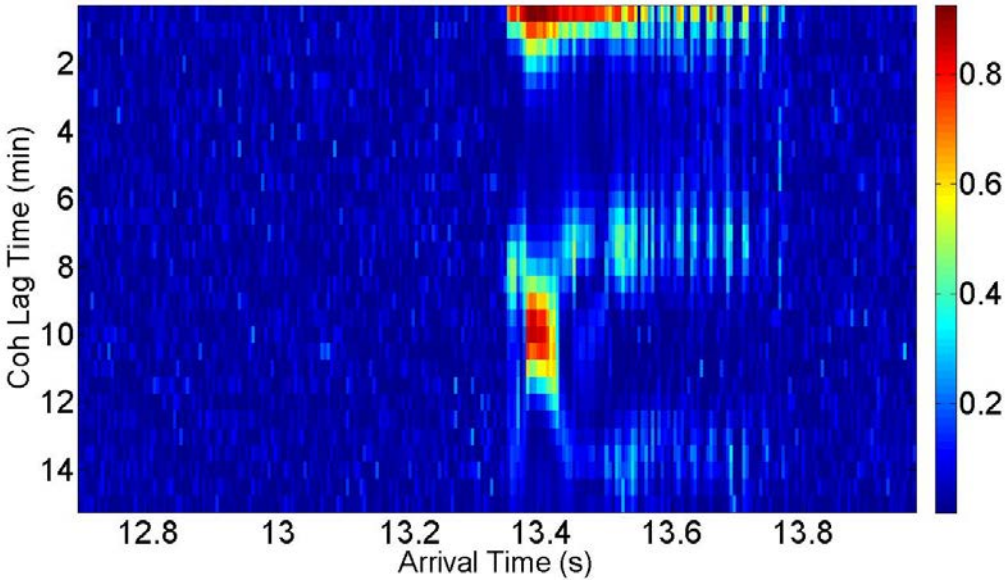

Figure 3.50: Figure shows coherence for the SIW band and center frequency 800 Hz.

All results are in very good agreement with the data. In the first band all modes are affected equally, and as the frequency is increased the modes coherence time decreases. Second band results show almost no coherence regardless of the frequency

used. This was expected since this band has very low coherence values due to noise. Here modes are distorted not translated. Third band results show a first mode very coherent at 100Hz and periods where we have canceling of the modes and others where we can see its reinforcement. Modes appeared to be in phase and out of phase. Forth band results show a very coherent first mode in figure 3.43, which fades as the frequency is increased. The last band, which is a narrow band within the third band, shows a similar result as we compare it to the ones we found in third band. The first mode is also vey coherent but here higher order modes appeared more coherent since noise was also reduced. Modes here are also translated sometimes in phase and other times in an uncorrelated way.

3.4.3 RANGE DEPENDENCE RESULTS

In this final section the range dependence of coherence between moorings SW 32, SW 45 and the shark array will be analyzed. Similarly as what was done in section 3.4.2 the data from SW 32 and SW 45 moorings will be analyzed and addressed in bands, with each band being used as an input for our model. The difference here is that we used three different sound speed profiles in range, one for each mooring, are used to calculate the coherence and to analyze the distortion/translation of the modes.

The distance in nautical miles between moorings is presented in Table 3.4:

Moorings	**Shark**	**SW32**	**SW45**
Shark	-	4.9 Mi	10.6 Mi
SW 32	4.9 Mi	-	5.7 Mi
SW 45	10.6 Mi	5.7 Mi	-

Table 3.4: Distance in nautical miles between moorings showed in Figure 3.51

Six thermistors were used for the SW 32 mooring and eleven for the SW 45. The data were demeaned and after dividing the power spectral density in bands a cosine bell filter was used to avoid any leakage. After that the temperature data was converted into sound speed using a routine in Matlab. Figure 3.51 shows the relative position between moorings.

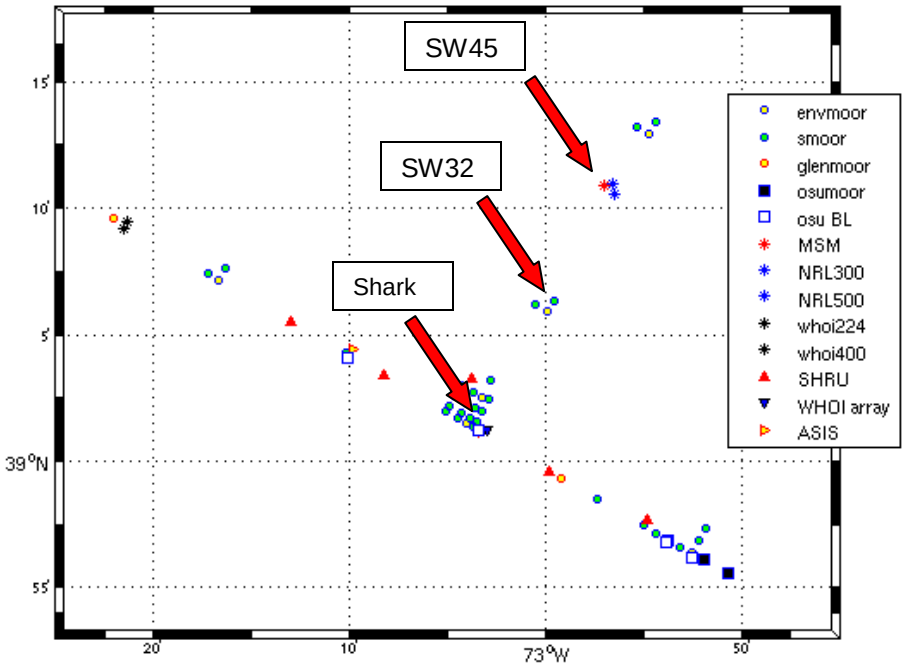

Figure 3.51: SW06 Chart with moorings and locations. Reprinted from Woods Hole Oceanog. Inst. Tech. rept., WHOI-2007-04.

Figures 3.52, 3.53 and 3.54 show the result for the first band at different center frequencies (100Hz, 200Hz and 400Hz).

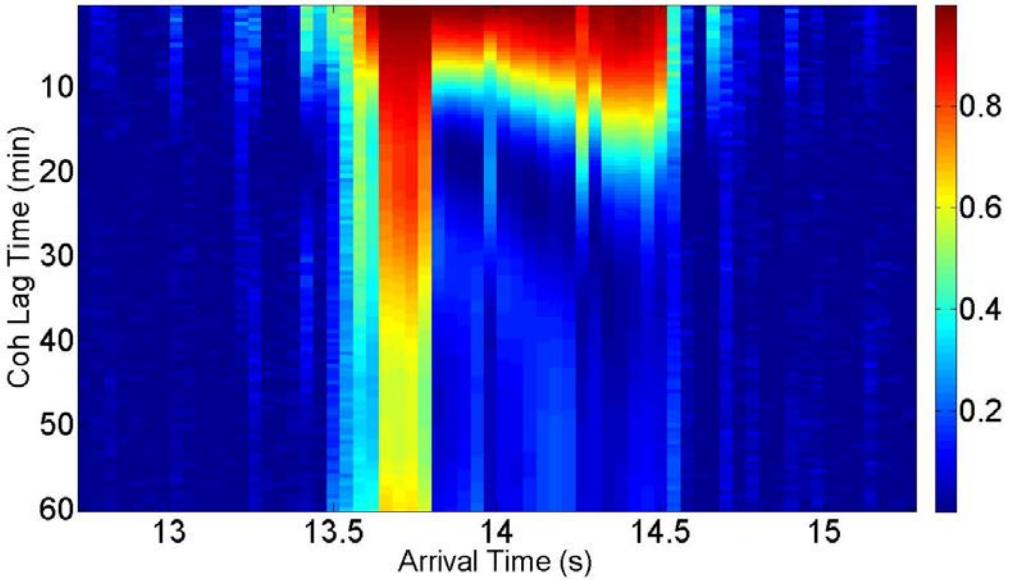

Figure 3.52: Figure shows coherence for the 1st band and center frequency 100 Hz.

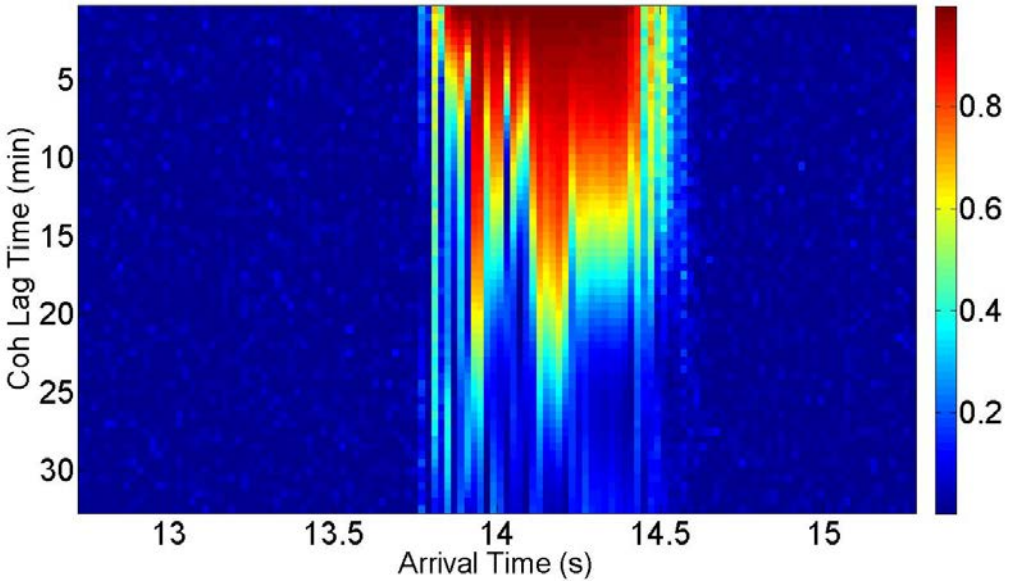

Figure 3.53: Figure shows coherence for the 1st band and center frequency 200 Hz.

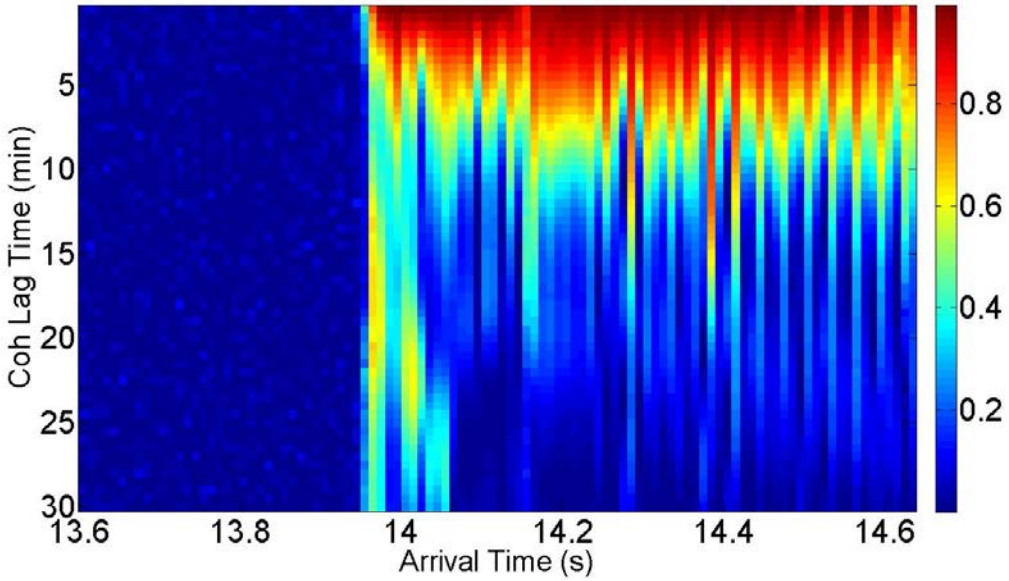

Figure 3.54: Figure shows coherence for the 1st band and center frequency 400 Hz.

Figures 3.55, 3.56, 3.57 and 3.58 show the result for the second band at different center frequencies (100Hz, 200Hz, 400Hz and 800Hz).

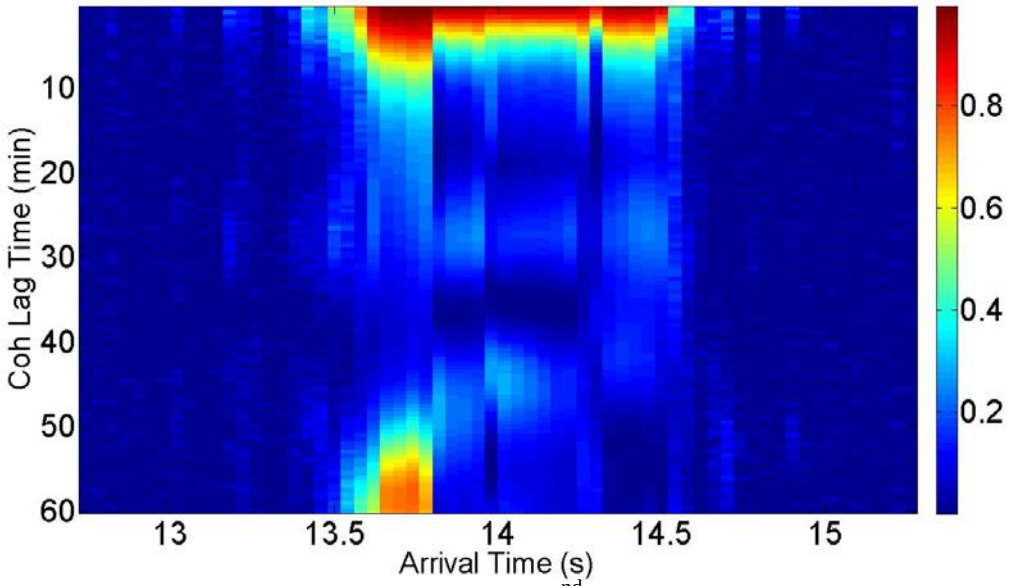

Figure 3.55: Figure shows coherence for the 2nd band and center frequency 100 Hz.

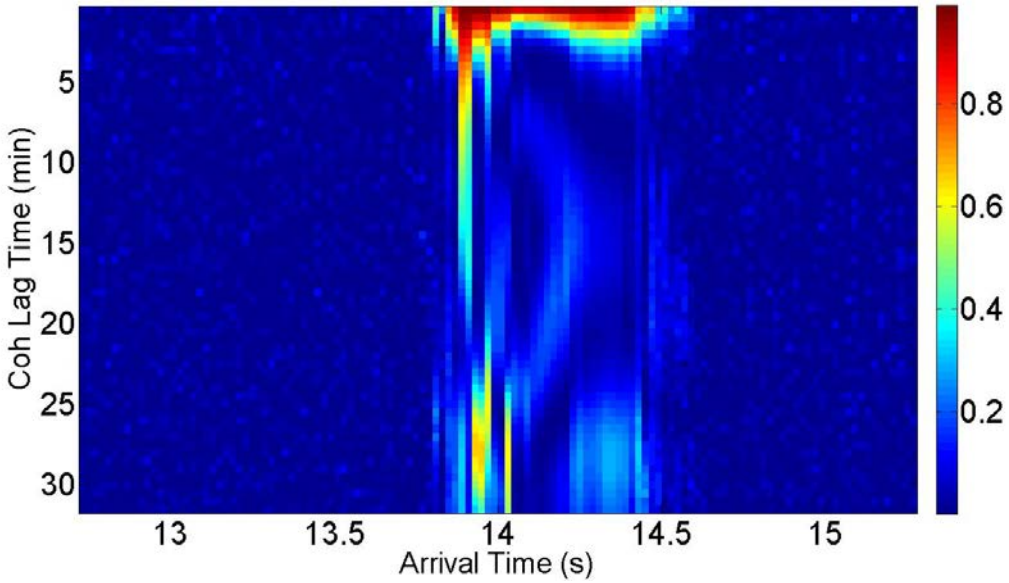

Figure 3.56: Figure shows coherence for the 2nd band and center frequency 200 Hz.

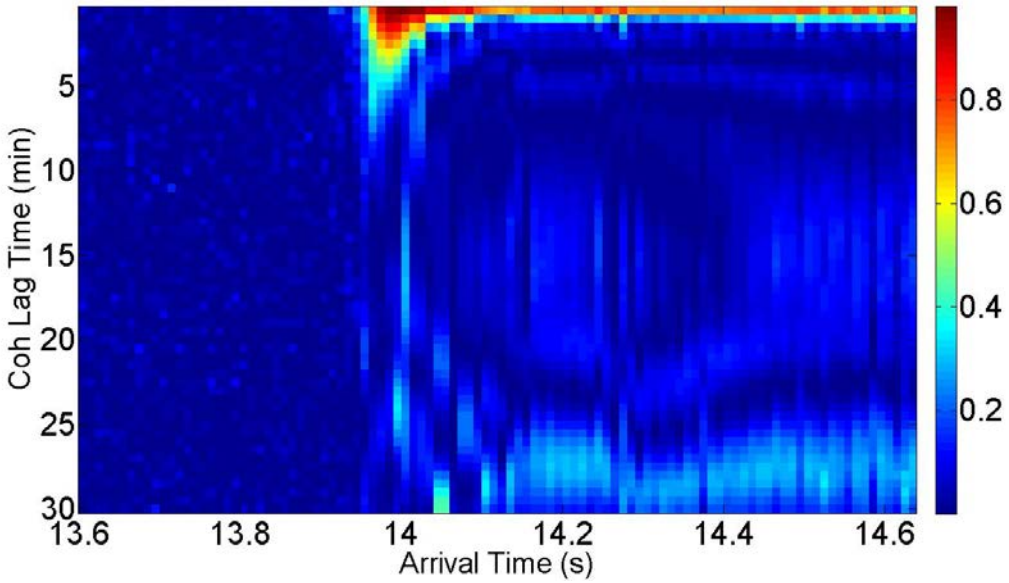

Figure 3.57: Figure shows coherence for the 2nd band and center frequency 400 Hz.

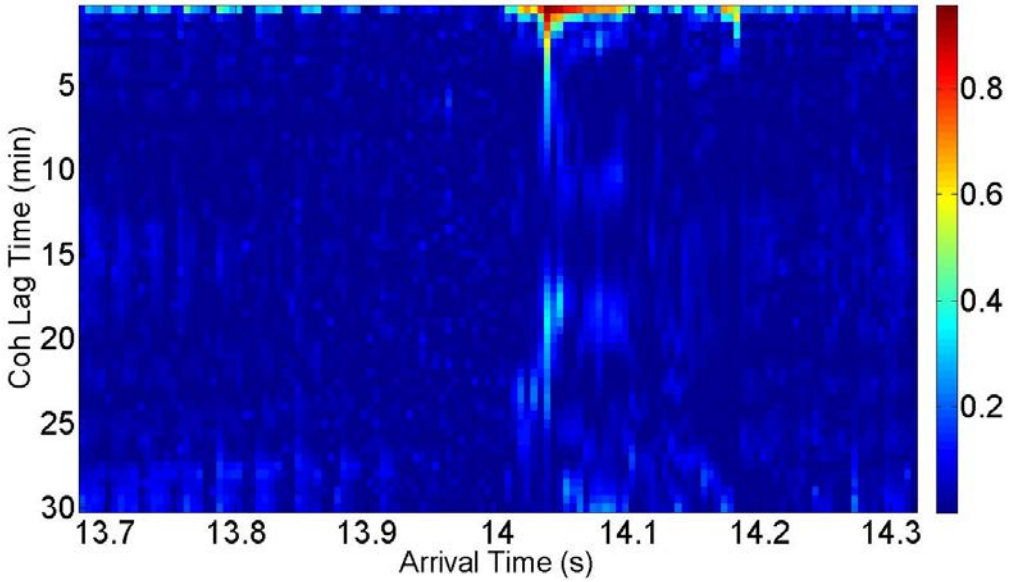

Figure 3.58: Figure shows coherence for the 2nd band and center frequency 800 Hz.

Figures 3.59, 3.60 and 3.61 show the result for the third band at different center frequencies (100Hz, 200Hz and 400Hz).

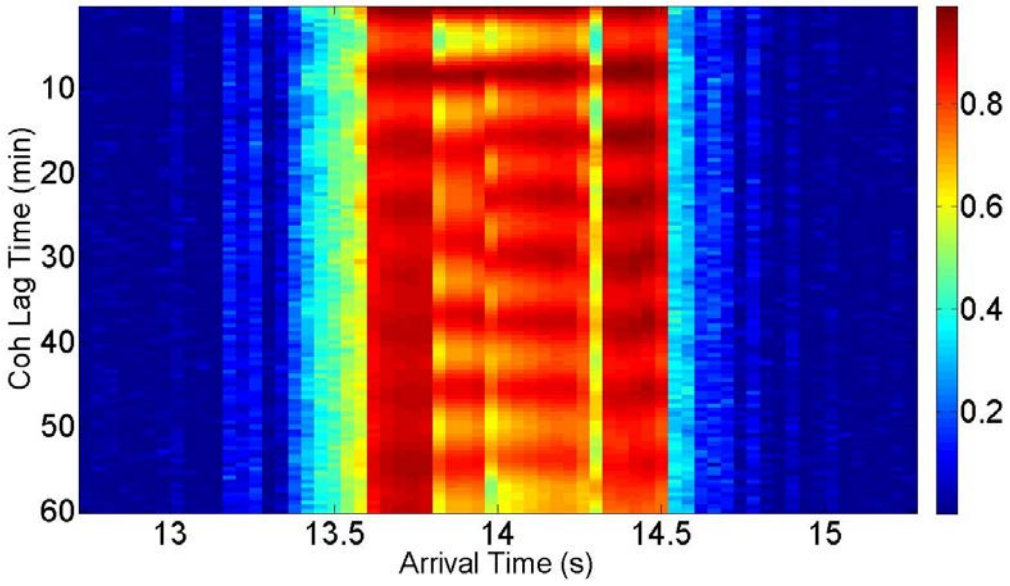

Figure 3.59: Figure shows coherence for the 3rd band and center frequency 100 Hz.

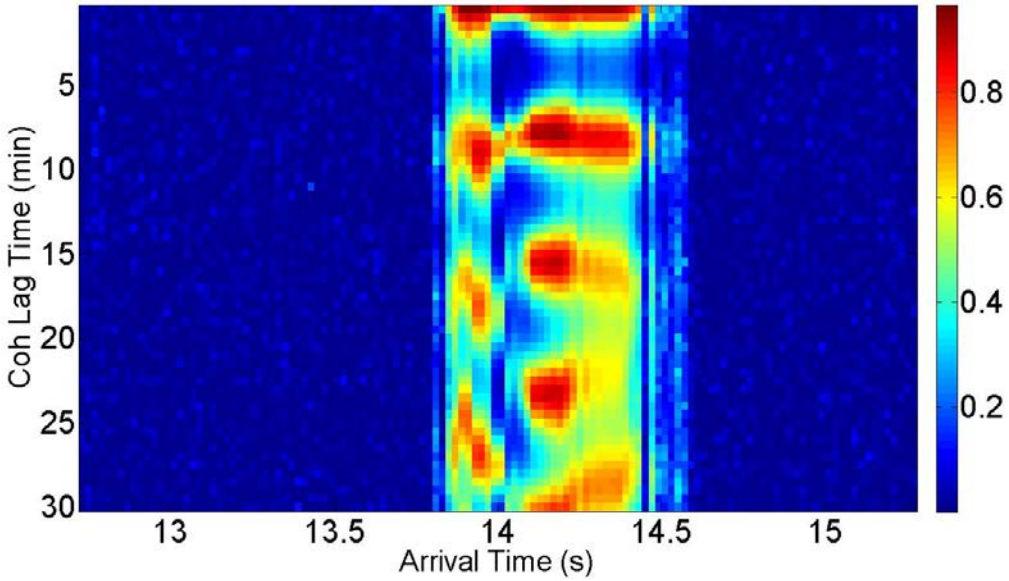

Figure 3.60: Figure shows coherence for the 3rd band and center frequency 200 Hz.

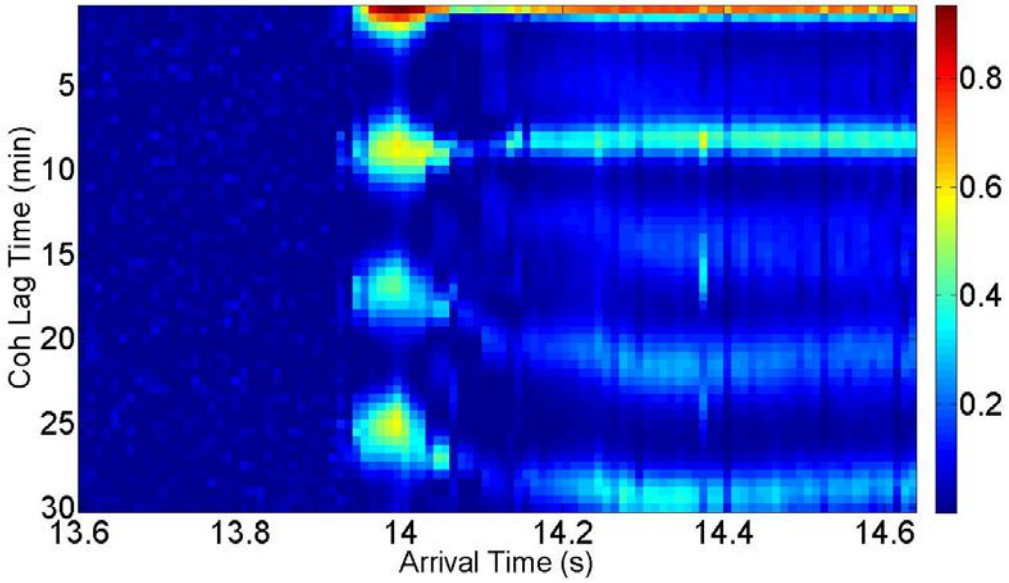

Figure 3.61: Figure shows coherence for the 3rd band and center frequency 400 Hz.

Figures 3.62, 3.63 and 3.64 show the result for the forth band at different center frequencies (100Hz, 200Hz and 400Hz).

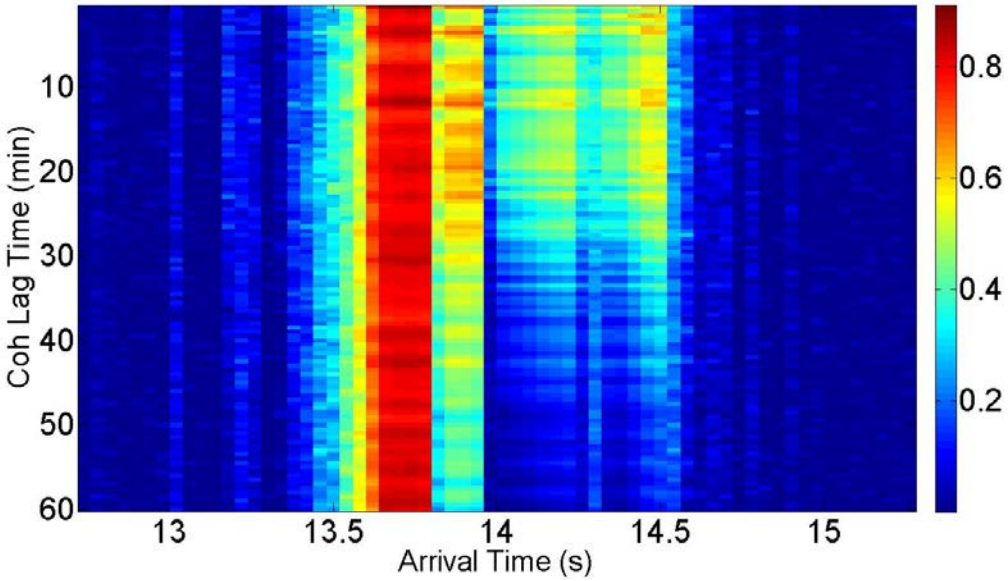

Figure 3.62: Figure shows coherence for the 4th band and center frequency 100 Hz.

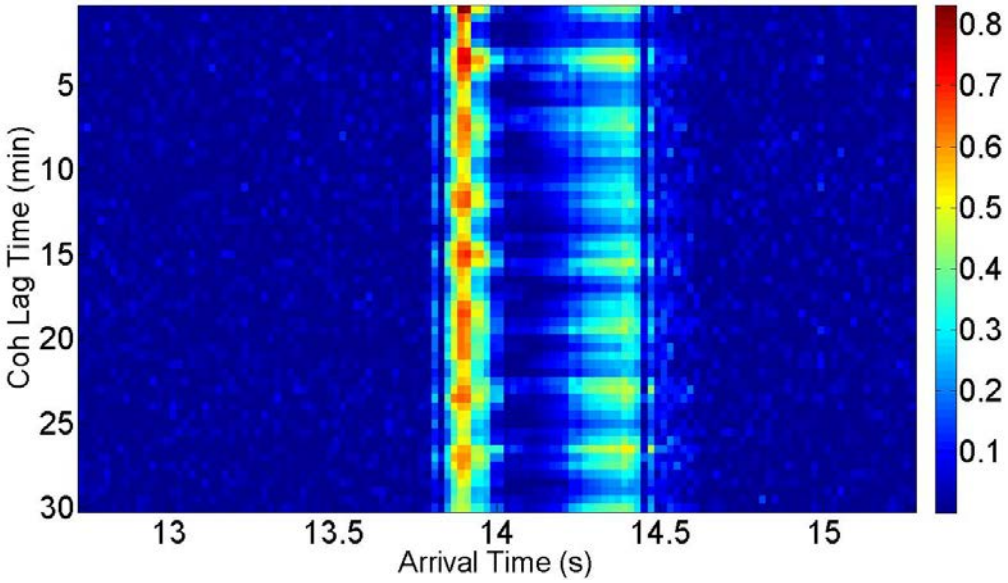

Figure 3.63: Figure shows coherence for the 4th band and center frequency 200 Hz.

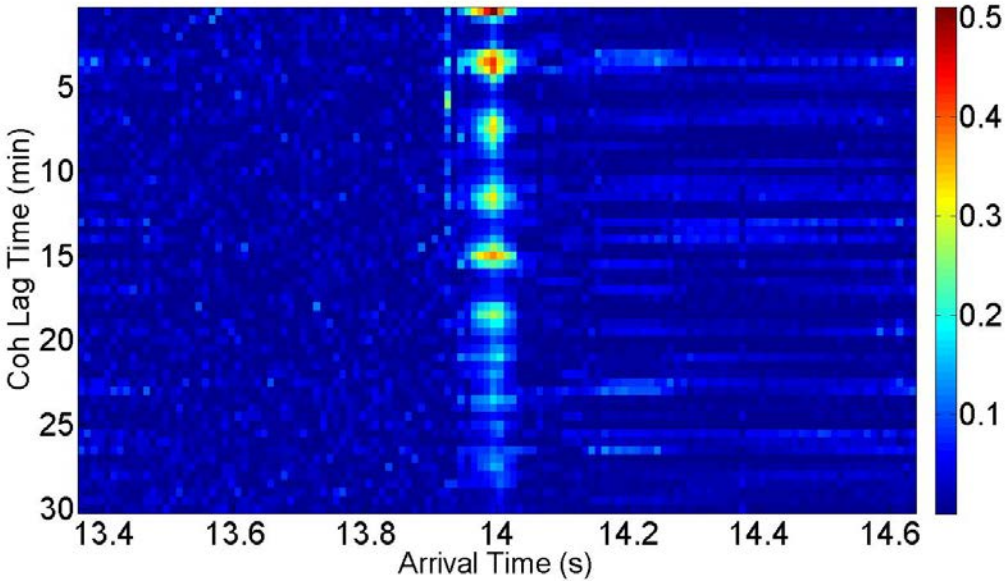

Figure 3.64: Figure shows coherence for the 4th band and center frequency 400 Hz.

Figures 3.65, 3.66, 3.67 and 3.68 show the result for the forth band at different center frequencies (100Hz, 200Hz, 400Hz and 800Hz).

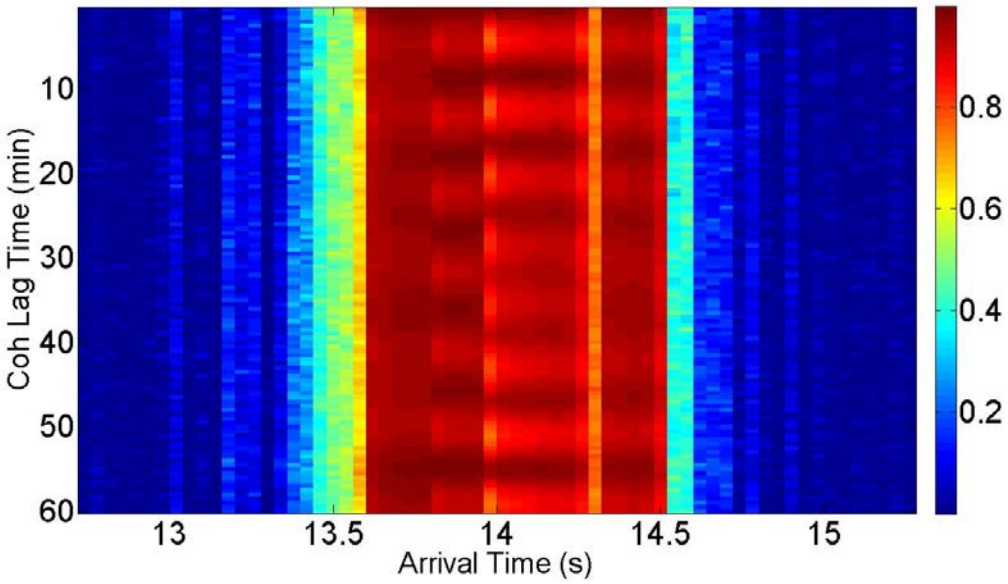

Figure 3.65: Figure shows coherence for the SIW band and center frequency 100 Hz.

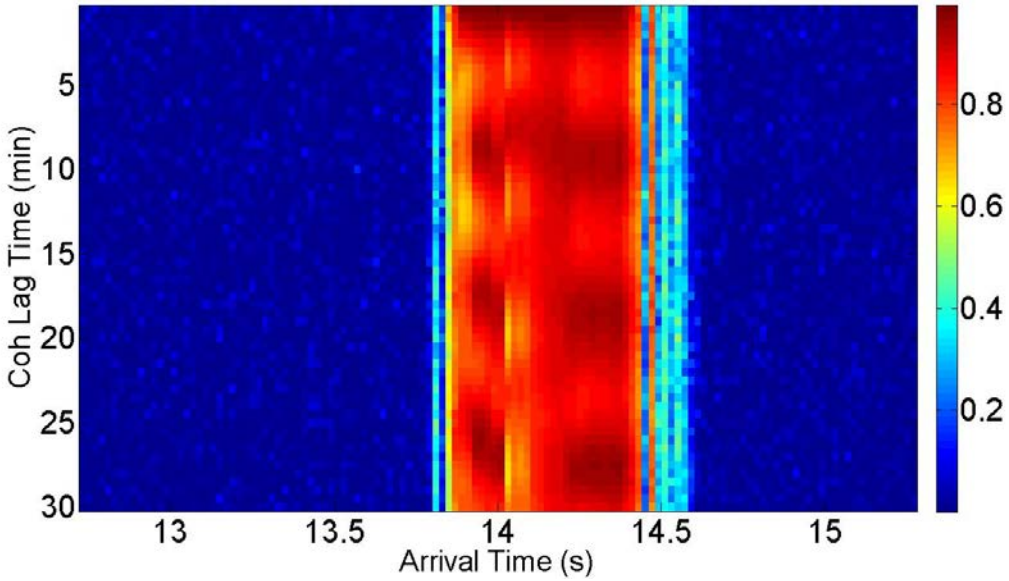

Figure 3.66: Figure shows coherence for the SIW band and center frequency 200 Hz.

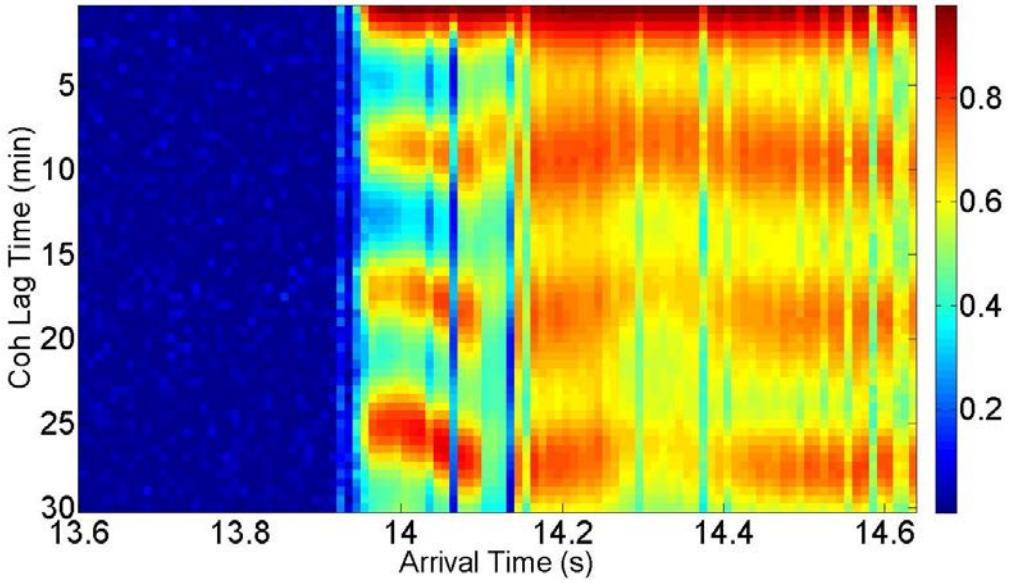

Figure 3.67: Figure shows coherence for the SIW band and center frequency 400 Hz.

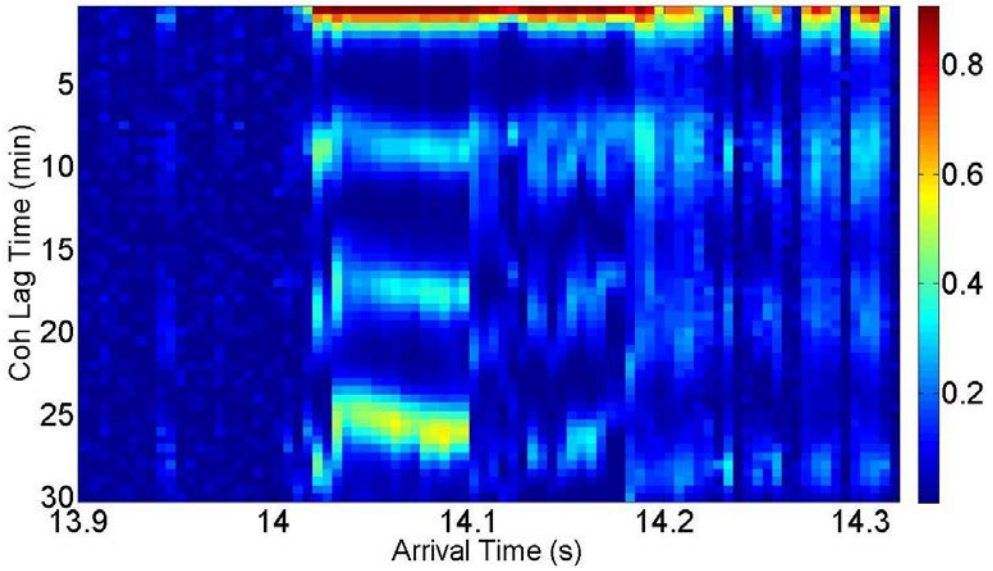

Figure 3.68: Figure shows coherence for the SIW band and center frequency 800 Hz.

CHAPTER 4

CONCLUSIONS AND FUTURE WORK

For many years, the research communities have focused on the effects of internal waves on temporal coherence; whereas, Navy applied programs are more concerned with the randomizing effect of the combination of bottom bathymetry variations and platform motion on array (spatial) coherence. It seems unlikely that it is possible to isolate these two causes in the shallow ocean. In the deep ocean and for propagation by refracted paths, one need only consider the effects of internal waves to understand coherence. But in shallow oceans, propagation is generally by reflected paths and bottom variability can and does affect coherence and often is more randomizing than internal waves. We have found that for very low frequencies the bottom appears flat and internal waves alone determine coherence. At very high frequencies we observed that the slightest sound speed variations randomize and de-correlate the signal even without internal waves.

Our approach has been to observe and model the coherence properties of individual mode arrivals. We find that understanding of mode properties holds promise of explaining and predicting both temporal and spatial coherence for fixed and moving platforms. The two distinct coherences, temporal and spatial, are related to the same mode properties. Stable clean modes result in temporal and spatial coherence but distorted and randomized modes result in loss of coherence - all predictable with physical models with appropriate random inputs for the medium and boundaries. Previous attempts by other investigators to model coherence using ray models were unsuccessful owing to chaos introduced by ray theory approximations.

An initial finding about internal waves is that the low end of the spectrum simple translates the unperturbed modes past the receiver without loss of phase coherence; but, higher frequencies distort mode shape in an unpredictable way that randomizes phase. The results are quantitative in that, spectral band that causes the randomness change with the acoustic frequency. Despite the high intense solitons observed during the experiment they do not affect the modes as much as thought. In fact, the effect is almost the same for all modes. But there are significant exceptions.

The results shown, without bottom variations, do not account for the observed mode dependence on coherence, i.e. the higher order modes having lower coherence. The lower spectral content of CIW, i.e. bands 1 and 2, have no influence on coherence calculations but higher bands do have a decorrelation effect on higher order modes. This effect can be explained by the fact that higher order modes propagate down the channel after reflections at the bottom and the surface. This way higher order modes are affected by the vertical fluctuations on the channel while the first mode propagates down the channel without refractions and as a consequence observing less fluctuations of the medium.

For the SIW case, the results show that even though these solitary internal waves are at higher frequencies, i.e. the same band as those of the CIW that does cause incoherence, they are so regular in space that no randomness and incoherence are introduced.

It has to be said that this thesis analyzed only the large scale sound speed structures. There is also much fine scale variations in both the vertical and the horizontal that were not taken into account in this work. The number of points used as inputs for

sound speed and range steps had to be constrained. As a result some of the small scale fluctuations could introduce some changes in the results or this could probably be a small scale effect.

Moreover, when comparing the experimental results and the model predictions it is clear that some of the mode dependence can be explained by the IW field. But not only. Bottom fluctuations are more important and play the main role deteriorating the acoustic modes and as a consequence the mode coherence.

As a future work, we are going to analyze data from the SW06 experiment using the MMPE model but this time introducing random bathymetry fluctuations. Another factor that we are going to analyze is how the ship motion contributes to loss of coherence and if possible at which speed the source motion becomes the driving factor in loss of coherence. Our objective in a near future is the systematic application of statistical properties describing the sound field and bottom to the models to completely account for observations. Mode coherence will be used to compute or otherwise estimate conventional temporal and spatial coherence. The end result will be a confirmed general theory that relates any observation of coherence to statistical properties of the medium and bottom for either fixed or moving platforms.

REFERENCES

Blatstein, I. M., Newman, A. V., and Überall H., 1973: A comparison of Ray Theory, Modified Ray Theory, and Normal Mode Theory for a deep ocean arbitrary velocity profile. J. Acoust. Soc. Am. Volume 54, Issue 1, 271-271 (1 page).

Collins, J. M., Duda, T. F., Lynch, J. F., and DeFerrari, H. A., 2008: Observed limiting cases of Horizontal coherence and array performance in a time-varying internal wave field. J. Acoust. Soc. Am., 124, EL 97-103.

DeFerrari, H. A., 2008: Observations of low-frequency temporal and spatial coherence in shallow water. J. Acoust. Soc. Am., 125(1), EL 45-49.

DeFerrari, H. A., Lynch, J. F., and Newhall, A., 2008: Temporal coherence of mode arrivals. J. Acoust. Soc. Am., 124(3), EL104-109.

Derzhavin, A. M., and Semenov, A. G., 2001: Sound fluctuations caused by Internal Waves in shallow sea. Acoustical Physics, 47(2), 169-177.

Duda, T. F., and Preisig, J. C., 1999: A modeling study of acoustic propagation through moving shallow water solitary wave packets. IEEE J. Ocean. Eng., 24, 16-32.

Gill, A. E., 1982: Atmosphere-Ocean Dynamics. Academic, London, pp 661.

Owen, S. L., 1960: Effect of an Internal Wave on sound in the ocean. J. Acoust. Soc. Am., 33(5), 677-681.

Owen, S. L., 1961: Observations on Internal Waves in shallow water. Limnology and Oceanography, 6(3), 312-321.

Palmer, D.R., Georges, T.M., and Jones, R.M., 1991: Classical chaos and the sensitivity of the acoustic field to small-scale ocean structure. Computer Physics Communications, Vol. 65, 219-223.

Preisig, J. C., and Duda, T. F., 1997: Coupled acoustic mode propagation through continental shelf internal solitary waves. IEEE J. Ocean. Eng., 22, 256-269.

Ren, Y., and Li, Z., 2010: Effects of internal waves on signal temporal correlation length in the South China Sea. Chinese Journal of Oceanology and Limnology, 28(5), 1119-1126.

Serebryany, N. A., Newhall, A., and Lynch, F. J., 2008: Observations of noise generated by nonlinear internal waves on the continental shelf during the SW06 experiment. J. Acoust. Soc. Am. 123, 3589.

Smith, K. B., Brown, M. G., and Tappert, F. D., 1991: Ray chaos in underwater acoustics. J. Acoust. Soc. Am., 91(4), 1939-1949.

Smith, K.B., "Convergence, stability, and variability of shallow water acoustic predictions using a split-step Fourier parabolic equation model," J. Comp. Acoust., Vol. 9, No. 1, pp. 243-285, 2001.

Song, A., Badiey, M., Newhall, A., Lynch, J. F., and DeFerrari, H. A., 2008: Effects of internal waves on acoustic coherent communications during SW06. Acoustics 08 Paris, 2845-2850.

Voronovich, A. G., and Ostashev, V. E., 2005: Low-frequency sound scattering by internal waves in the ocean. J. Acoust. Soc. Am., 119(3), 1406-1419.

Yang, J., and Roussef, D., 2010: Effect of the Internal Tide on acoustic transmission loss at midfrequencies. IEEE J. Ocean. Eng, Vol. 35 (1), 3-11.

Yang, T. C., 2006: Measurements of temporal coherence of sound transmissions through shallow water. J. Acoust. Soc. Am., 120(5), 2595-2614.

Y.-T. Lin , A. E. Newhall , T. F. Duda , P. F. J. Lermusiaux and P. J. Haley: Statistical merging of data sources to estimate full water-column sound speed in the New Jersey Shallow Water 2006 Experiment, IEEE J. Ocean. Eng.